Input-specific bi-directional regulation of CA3 pyramidal cell excitability: its implications in sequence learning

Kisang Eom[1,3] Yujin Kim[1,2], Seungmin Baek[1], Alan J Park[1], Won-Kyung Ho[1], Suk-Ho Lee[1,2,4*]

[1] Department of Physiology, Seoul National University College of Medicine, 103 Daehak-ro, Jongno-gu, 03080, Seoul, Republic of Korea.

[2] Department of Brain and Cognitive Science, Seoul National University College of Natural Science, 103 Daehak-ro, Jongno-gu, 03080, Seoul, Republic of Korea.

[3] Current address: Department of Physiology, Keimyung University School of Medicine, 1095 Dalgubeol-daero street, Dalseo-gu district, Daegu, Republic of Korea.

[4]Corresponding author

*Correspondence: Suk-Ho Lee: leesukho@snu.ac.kr

Acknowledgements:

This study was supported by National Research Foundation of Korea (Grant/Award Number to SHL, 2020R1A2C2006438).

Abbreviations

A/C, associational/commissural; Ach, acetylcholine; CA3-PC, CA3 pyramidal cell; CaTs, Ca^{2+} transients; CFC, contextual fear conditioning; CREB, cAMP response element binding protein; E-S, EPSP-to-spike; fEPSP, field EPSP; G_{in}, input conductance; GSH, reduced form of glutathione; KO, knock-out; LTP-IE, long-term potentiation of intrinsic excitability; MF, mossy fiber; PIE, potentiation of intrinsic excitability; PP, perforant pathway; PTK, protein tyrosine kinase; PTP, protein tyrosine phosphatase; SC, somatic conditioning; shEGFP, short-half life EGFP; WCR, whole-cell recording

Abstract

Neuronal excitability is a key determinant for recruitment of a neuron to an ensemble. High-frequency mossy fiber (MF) inputs induce a prolonged increase in the excitability of a CA3 pyramidal cell (called long-term potentiation of intrinsic excitability, LTP-IE), thereby weak perforant pathway (PP) inputs can induce long-term potentiation at PP synapses (PP-LTP). However, sustained hyperexcitability is detrimental, and a mechanism to reverse this primed state is necessary. Here, we show that burst firings of CA3 pyramidal cells elicited by PP or recurrent synaptic inputs reverse the MF-induced LTP-IE. Moreover, the high-frequency PP inputs to MF-primed CA3 pyramidal cells induced not only PP-LTP but also restored the high excitability state. Labeling a neuronal ensemble using c-fos promoter in animals exposed to a novel context, we found most CA3 ensemble cells exhibited increased excitability, indicative of LTP-IE. Moreover, when the animals experienced novel contexts twice with an interval, a substantial subset of putative twice-activated CA3 ensemble cells exhibited reduced excitability, implying depotentiation of LTP-IE. We developed an in silico model based on these experimental results and found that MF-induced LTP-IE and its depotentiation are critical for association of orthogonal neuronal ensembles representing temporally discontiguous events.

Keywords

CA3 pyramidal cell; intrinsic excitability; depotentiation; neuronal ensemble; computational modelling; sequence learning

Highlights

- It is unknown how non-overlapping ensembles are linked in the hippocampal CA3 area.
- Mossy fiber inputs prime CA3 pyramidal cells by enhancing dendritic excitability.
- Perforant pathway (PP) inputs to the primed cells induce synaptic strengthening.
- At the same time, the high excitability state is restored by PP inputs.
- This learning rule may play a key role in sequence learning in CA3 network.

Introduction

Hippocampal CA3 pyramidal cells (CA3-PCs) receive two kinds of extrinsic synaptic inputs from dentate gyrus and entorhinal cortex via mossy fibers (MFs) and perforant pathway (PP), respectively. Sparse and strong non-Hebbian MF inputs contribute to orthogonal encoding, while weak and a larger number of Hebbian PP inputs are required for cued memory retrieval of a pattern stored in the CA3 recurrent network (Treves and Rolls 1992; O'Reilly and McClelland, 1994; Lee & Kesner, 2004). Involvement of PP synapses in retrieval of episodic memory implies that long-term plasticity (LTP) at PP synapses would play a key role in triggering reactivation of CA3 ensembles from auto-associative CA3 network during cued retrieval. Because PP synaptic inputs are not strong enough to drive firing of CA3-PCs, MF-driven firing would be required for induction of Hebbian LTP at PP synapses (McNaughton and Morris, 1987). High frequency MF inputs not only provide such immediate depolarization but also induce sustained enhancement of dendritic voltage responses to PP synaptic inputs, called long-term potentiation of intrinsic excitability (LTP-IE) (Eom et al., 2019; Hyun et al., 2015; Hyun et al., 2013). The MF-induced LTP-IE is mediated by an increase in the distal apical dendritic excitability (Hyun et al., 2013), and potentiates the EPSP-to-spike (E-S) coupling of PP inputs (E-S potentiation) (Hyun et al., 2015). Therefore, high-frequency MF inputs prime a CA-PC for homosynaptic LTP at PP synapses (PP-LTP) because the E-S potentiation lowers the threshold of PP input strength required for induction of PP-LTP (called LTP threshold) (Eom et al. 2022). Given that LTP-IE is not a synapse-specific process but occurs over a whole distal dendritic arbor (Hyun et al., 2013), LTP-IE without depotentiation would lead to rapid saturation of PP-CA3 synaptic weights, which will impair further learning (Moser et al., 1998), and excitation/inhibition imbalance of the CA3 recurrent network. It remains unexplored, however, how MF-induced high excitability state of CA3-PC is restored to the baseline.

The other question to be addressed is whether LTP-IE indeed occur in CA3-PCs that participate in neuronal ensembles (called CA3 ensemble cells) *in vivo*. This question is crucial to understand CA3 ensemble dynamics because neuronal excitability is a key factor that determines whether a given neuron is recruited to an ensemble carrying information. Once a CA3-PC receives high-frequency MF inputs and undergoes LTP-IE in a previous episode, the probability for the primed cell to be recruited to an ensemble in the next episode would be enhanced because E-S potentiation would enable PP input alone to drive firing in the primed CA3-PC. Whereas dynamic changes of intrinsic excitability accompanied with

behavioral learning have been explored in hippocampal DG and CA1 area (Oh & Disterhoft, 2015; Pignatelli et al., 2019),the same issue in the CA3 region remains unexplored.

The present study was set out to address these two questions. Here, we show that MF input-induced primed state of a CA3-PC is terminated by high-frequency PP or associational/commissural (A/C) inputs. Moreover, CA3 ensemble cells exhibited indeed high excitability features similar to CA3-PCs that underwent LTP-IE, and LTP-IE was reversed in a subset of putative twice-activated CA3 ensemble cells when an animal experienced two temporally separated events. Incorporating in vitro findings to the Hebb-Marr CA3 network model (McNaughton & Morris, 1987), we propose that the MF- and PP-induced bi-directional regulation of CA3-PC excitability may link two orthogonal ensembles representing two events adjacent in a sequence even if they are temporally separated.

Materials and Methods

Animals and ethical approval. All studies, experimental protocols, and animal manipulation protocol described in this article were conducted with the Institutional Animal Care and Use Committee (IACUC). The animals were maintained in standard environmental conditions (Temperature: 25 ± 2 ºC, Humidity: 60 ± 5 %, Dark/Light cycle: 12/12h) and monitored under veterinary supervision by Institute for Experimental Animals, Seoul National University College of Medicine.

Preparation of hippocampal slices. Acute transverse hippocampal slices were obtained from Sprague-Dawley rats (PW2-3 for Figures 1-4 and Figures S2-S3; PW6 for Figure 5; PW, postnatal weeks) or cfos-shEGFP mice (PW6-8 for Figures 6-7) or ZnT-heteroKO and ZnT-heteroKO/cfos-shEGFP mice (PW6, Figure 8) of either sex. Animals were anesthetized by inhalation of isoflurane. After decapitation, brain was quickly removed and chilled in ice-cold preparation solution containing 75 sucrose, 87 NaCl, 25 $NaHCO_3$, 2.5 KCl, 1.25 NaH_2PO_4, 25 D-glucose, 7 $MgCl_2$, and 0.5 $CaCl_2$ (in mM; equilibrated with carbogen mixture of 95% O_2 and 5% CO_2). After mounting on a slicer (Leica VT1200, Nussloch, Germany), 300 µm (whole-cell recording)-thick transverse slices (whole-cell recording) were prepared and incubated at 34 ºC for 30 min in the preparation solution, and thereafter stored at room temperature (22 ºC). For experiments, slices were transferred to a submersion recording chamber superfused with standard aCSF containing 124 NaCl, 26 $NaHCO_3$, 3.2 KCl, 1.25 NaH_2PO_4, 10 D-glucose, 2.5 $CaCl_2$, and 1.3 $MgCl_2$ (in mM).

111 **Electrophysiological study.** Whole-cell voltage- or current-clamp recordings from CA3-PCs were
112 performed at near-physiological temperature (34 ± 1 ºC), while the recording chamber was perfused with
113 the standard aCSF at 1 ~ 1.5 ml/min. Patch pipettes were pulled from borosilicate glass tubing (outer
114 diameter: 1.5 mm, wall thickness: 0.225 mm) with a horizontal pipette puller (P-97, Sutter Instruments,
115 Novato, CA, USA) and filled with the intracellular solution containing 130 K-gluconate, 7 KCl, 1 $MgCl_2$, 2
116 Mg-ATP, 0.3 Na-GTP, 10 HEPES, 0.1 EGTA (in mM; pH adjusted to 7.20 with KOH, 295 mOsm) with the
117 pipette resistance was 3 ~ 4 MΩ. After formation of whole-cell configuration on the somata of CA3-PCs,
118 recordings were performed from only those cells that had stable resting membrane potential within -76
119 and -58 mV (cells that had more positive resting membrane potential or unstable resting membrane
120 potential were discarded). Under this condition, input conductance (G_{in}) was measured from subthreshold
121 voltage responses to -30 pA and +10 pA current steps of 0.5 s (Hyun et al., 2015). G_{in} was monitored every
122 10 s before and after delivery of a conditioning protocol. Recordings were obtained in the presence of a
123 $GABA_A$ receptor antagonist, picrotoxin (PTX, 100 µM) unless specified. All recordings were made using a
124 MultiClamp 700B amplifier controlled by Clampex 10.2 through Digidata 1440A data acquisition system
125 (Molecular Devices, Sunnydale, CA, USA). Also, we stimulated different types of synapses on CA3-PCs to
126 evaluate the influence of each synaptic input on the intrinsic excitability of CA3-PCs. Afferent PP fibers
127 were stimulated with a concentric bipolar electrode (CBAPB125; FHC Inc., Bowdoin, ME, USA) positioned
128 at SLM on the border of the subiculum and CA1 (for PP stimulation)(Perez-Rosello et al., 2011).
129 Associational/commissural (A/C) fibers were stimulated with a glass micro-pipette placed on alveus. Brief
130 stimulation pulses (0.1 ms) were generated by a computer-controlled digital stimulator (DS8000, WPI;
131 Sarasota, FL, USA) and delivered to a stimulation electrode through an isolation unit (DLS100 stimulus
132 isolator, WPI). For extracellular recording, field excitatory postsynaptic potentials (fEPSPs) were recorded
133 from striatum lacunosum-moleculare (SLM) of CA3 by a glass electrode filled with 150 mM NaCl
134 (resistance, c.a. 1 MΩ).

135 Prior to electrophysiological studies, an incision was made along the hippocampal sulcus of the slice to
136 prevent possible contamination of indirect cortical input as in our previous study (Hyun et al., 2015). The
137 stimulation intensity was adjusted so that the value of PP-EPSC was 10-20 pA in the whole cell
138 configuration (Figs. 1, 3, 4 and 7). For extracellular recordings, the PP stimulation intensity was adjusted
139 such that synaptic responses were lower than 20% of the maximum intensity that does not elicit
140 population spikes (10 – 30 V, Fig. 2). For the alveus stimulation, the optimal stimulation position was found
141 by moving the glass electrode on the slice, and the stimulation intensity was 3-5V (Fig. 2-3). For the MF

142 stimulation (Figs. 2 and 4), we adopted minimum stimulation protocol, by which the failure rate was about
143 40-60% (c.a. 30 V at dentate gyrus granule cell layer; Hyun et al., 2015, Jonas 1993).

144 **Stereotaxic surgery and intrahippocampal injection of adeno-associated virus (AAV) for ex vivo study.**
145 An adeno-associated virus (AAV-RAM-d2TTATRE-EGFP-WPRE-pA, titer: 4.8 × 10^{12} GC/ml) was
146 manufactured by KIST virus facility (Seoul, Republic of Korea). Surgery was performed on young-adult SD
147 rats (6 weeks). Before stereotaxic injection of the AAV into hippocampus, animals were singly housed to
148 new homecage for 1 week to acclimation with doxycycline diet (40 mg/kg). Animals were kept on the
149 doxycycline diet and allowed to recover for at least 7 days following surgery. After anesthesia with
150 isoflurane, rats were secured in a stereotaxic frame (Neurostar, Tubingen, Germany). Holes were drilled
151 bilaterally in the skull at the injection sites (2 sites). Stereotaxic coordinates used for intrahippocampal
152 injections were as follows (from bregma); for a ventral hippocampus, anterior–posterior -2.85 mm,
153 mediolateral ±2.8 mm, dorsoventral 3.3 mm. A 33-gauge needle attached to a 50 µl Hamilton syringe
154 (#80908), mounted to the stereotaxic frame, and under control of a microinjection syringe pump UMP3T-
155 1 controller (WPI, Sarasota, FL, USA) was used to inject 0.8 µl of AAV at each site. Injections occurred at a
156 rate of 0.08 µl/min, after which the needle was left in place for an additional 2 min. After injections were
157 completed, the skin was sutured and the animals were allowed to recover for 1 h on a heating pad before
158 returning to the home cage. Mice remained in the homecage for an additional 2 weeks to recover before
159 the start of behavioral testing and post-hoc *ex vivo* experiments. The diet was switched to doxycycline-
160 free diet 2 days before contextual fear conditioning (CFC) to allow tetracycline transcriptional activator
161 (tTA) to activate the tTA-responsive element (TRE) promoter driving expression of EGFP.

162 **B6.Cg-Tg(Fos-tTA,Fos-EGFP*)1Mmay/J mice.** cfos-tTA/cfos-shEGFP mice were purchased from Jackson
163 laboratory (stock No: 018306; Donating investigator: Mark Mayford, The Scripps Research Institute, La
164 Jolla, CA), and crossed to the C57BL/6J background to maintain lineage. The cfos-shEGFP transgenes
165 allows us to quantify c-fos expression correlated with neuronal activation by measuring fluorescence of
166 short half-life green fluorescent protein (shEGFP, $t_{1/2}$ = 2 hours). For genotyping, DNA was isolated from
167 the tail of each mouse in the litter aged 6 ~ 8 days as the method provided by the Jackson Laboratory
168 (https://www.jax.org/strain/018306). All animals were maintained in the standard environmental
169 conditions described above.

170 **Exposure of animals to a novel context.** The cfos-tTA/cfos-shEGFP mice (hereafter cfos-EGFP mice) of
171 either sex (6-8 weeks old) were singly housed for 1 weeks before the experiments. On the experimental

172 day, the mice were placed in novel contexts; context A or A and B. Context A is a chamber (18 cm wide ×
173 18 cm long × 30 cm high; H10-11M-TC; Coulbourn Instruments 5583, PA 18052, USA) consisting of a metal
174 grid floor, aluminum side walls, and a clear Plexiglass front door and back wall. The context A chamber
175 was lit indirectly with a 12 W light bulb. The features of context B were the same as context A, except for
176 a unique odor (1% acetic acid), dimmer light (50% of A), and a slanted floor by 15° angle. The chamber
177 and cage were cleaned using 70% ethanol before placing an animal and between each runs. In context A,
178 but not in context B, animals were allowed a 3-min exploration, received a single foot shock (0.7 mA, for
179 2 s) and were returned to their home cage 60 s after the shock. In the context B, animals were allowed a
180 5-min exploration and returned to their homecage.

181 **Confocal microscopy and image quantification.** We tested 4 cfos-shEGFP mice (PW6-8) between 8 and
182 14 weeks of age for contextual exposure. Before the experiments, mice were a singly housed to new
183 homecage for 1 week for acclimation. For experiments depicted in Fig. S4, mice were divided into two
184 groups: exposure of context A only and waiting in homecage for 90 min (ctxA), exposure of context A and
185 B with 25-min interval and waiting in homecage for 60 min (ctxAB). Two groups were sacrificed to prepare
186 hippocampal slices after 90 min from the exposure of ctxA, as aforementioned. Confocal images from the
187 hippocampal slices in Fig. S4 were obtained in the submerged recording chamber that was continuously
188 perfused with the recording solution at 1.5 ml/min. To suppress unnecessary neural activity, picrotoxin
189 (10 µM) and CNQX (10 µM) were added to the solution. For analysis of fluorescence intensity of shEGFP(+)
190 CA3-PCs, Z-series (60-90 frames, 0.71 µm /frame) image were acquired from the live slices using a 40x
191 lens using FV 1200 confocal laser scanning microscope (Olympus, Tokyo, Japan). LD473 (15mW) laser
192 system controlled by combiner (FV10-MCPSU) was used to excite shEGFP in CA3-PCs. Typically, four
193 images were analyzed for each animal in the CA3 region. Fluorescence intensity profile for each shEGFP(+)
194 CA3-PCs based on depth from surface of slices were obtained from Z-stack image of CA3 region. The
195 surface of hippocampal slices was defined as 0 µm of depth in hippocampal slices. We regarded
196 fluorescence signals that is above a threshold of 5× the SD of baseline fluctuation of signal intensity profile
197 as the signal of shEGFP(+) CA3-PCs. The depth for the maximal fluorescence intensity was defined as the
198 depth of CA3-PCs.

199 **Epifluorescence imaging for AAV-injected rats or cfos-shEGFP mice.** Fig. 5 and 6 ~ 8 depict ex vivo
200 electrophysiological studies of CA3-PCs obtained from AAV-injected rats and cfos-shEGFP mice,
201 respectively. After acclimation of 1 weeks, AAV-injected rats were exposed to context A once for 5 min
202 and returned to homecage for 1, 1.5, and 3 hours (Fig. 5) and sacrificed to obtain brain slices. cfos-shEGFP

203 mice were divided into several groups: exposure of context A only and waiting in homecage for 60 min
204 (ctxA60), exposure of context A only and waiting in homecage for 90 min (ctxA90), and exposure of
205 context A and B with 25-min interval and waiting in homecage for 60 min (ctxAB). ctxA60 and ctxA90
206 groups were sacrificed to prepare brain slices after 60 min and 90 min from the exposure of context A.
207 For ctxAB group, animals were sacrificed to obtain brain slices after 60 min from the exploration of last
208 context, context B. EGFP or shEGFP was excited at 488 nm light with a monochromator (Polychrome IV,
209 xenon-lamp based, Polychrome-V, TILL-Photonics, Martinsried, Germany) and visualized using a 520/535-
210 nm band-pass emission filter (Fig. 5 and 6). In experiments for Fig. 6 - 8, to adjust deviation of fluorescence
211 intensity of shEGFP caused by the optical path length, 50 μM Alexa flour 594 (AF594) was added to
212 intracellular solution and loaded to CA3-PCs during whole-cell configuration. AF594 was excited at 594
213 nm light with the monochromator and visualized using a 660 nm long-pass emission filter. Acquired
214 images were analyzed with HC-Image Live 4.0 (Hamamatsu Photonics, Shizuoka, Japan). Whole-cell
215 recordings (WCR) were performed under the IR-DIC (Fig. 5Ab). WCR of EGFP(-) cells were used as control
216 and compared to recording of EGFP(+) or shEGFP(+) cells. The fluorescence intensity in the wide-field
217 epifluorescence image was set with manually-adjusted ROI based on the contour of cells.

218 **Simulation methods.** We considered a recurrent network comprised of 1000 PCs and 200 INs, in which
219 PCs and INs are numbered with indices from 1 to 1000, and those from 1001 to 1200, respectively. Initial
220 connectivity matrix (*W*) are shown in Fig. S7A. The connectivity, defined as the probability that an element
221 of *W* has nonzero value, was set to 10% for synaptic connections between PCs, while the connectivity
222 between CA3 PCs is less than 2% *in vivo* (Guzman et al., 2016). This high connectivity partially compensates
223 lower recurrent synaptic inputs from a given ensemble compared to the real rat CA3 network. The firing
224 property of neurons was simulated by the leaky integrate and fire model as described in detail elsewhere
225 (Yoon et al., 2020). The resting membrane potential (V_L) and the firing threshold (V_θ) were set to -65 and
226 −55 mV, respectively, for both CA3-PCs and GABAergic interneurons (INs). To model recurrent and
227 inhibitory synaptic inputs, we assumed that firing of a presynaptic CA3 PC or IN (denoted by subscripts 'e'
228 and 'i', respectively) induces an instantaneous increase in the postsynaptic conductance by G_s after a
229 synaptic delay, D_s, where $s \in \{e, i\}$ (D_e = 2 ms; D_i = 1 ms), and that the decay of the conductance change
230 follows a mono-exponential function with a time constant τ_s ($\tau_e = \tau_i$ = 10 ms) (Guzman et al., 2016; Kohus
231 et al., 2016). Multiple synaptic inputs to a neuron, *j*, were linearly summated. When the number of *s* type
232 presynaptic neurons innervating postsynaptic neuron, *j*, is K_s, the dynamics of subthreshold membrane
233 potential of the neuron, *j*, is assumed to follow the equations:

$$\tau_m \, dv_j(t)/dt = -(v_j - v_L) - (1/G_m) \; \Sigma_{s=\{e,i\}} \Sigma_{k=(1..Ks)} \; [G_{s,jk} \, (v_j - E_s) \; S_{s,jk}]$$

$$\tau_s \, dS_{s,jk}/dt = - S_{s,jk} + \Sigma_{t_{AP}} \, \delta(t - t_{AP} - D_s)$$

, where τ_m = cell membrane time constant; G_m = passive membrane conductance (5 nS for PCs and INs); $G_{s,\,jk}$ = synaptic conductance of synaptic type, *s*, from a neuron *k* to *j*; E_s = reversal potential of synapse type (E_e = 0 mV, E_i = -68 mV). The $S_{s,jk}$ is an activation parameter for synaptic type *s* from a neuron *k* to *j*. It is activated by presynaptic firing at t_{AP}, and undergoes mono-exponential decays with a time constant, τ_s. When membrane potential (*v*) surpasses the threshold potential (V_θ), the *v* was reset to -55 mV. To simulate a post-spike refractory period, the V_θ was increased to -15 mV just after firing, which undergoes mono-exponential decay with time constants of 50 and 15 ms for PC and INs, respectively. The summation of external excitatory synaptic inputs via MF and PP were calculated in the same manner as recurrent excitatory inputs, but the arrival of external synaptic inputs was pre-determined as a patterned input as shown in Fig. 8Ba. We assumed that four input patterns arrive at t = 0, 0.8 s, 1.8 s and 3 s in a series. The synaptic conductance values for MF and PP inputs to PCs were set to 20 and 0.3 nS, and those to INs were 4 and 0.15 nS, respectively. The decay time constants of MF and PP inputs were set to 4 and 17 ms (Hyun et al., 2015; Jonas et al., 1993). At the start of simulation, membrane potential of all neurons was initialized to -65 mV. The voltage derivative (dv/dt) of each neuron was calculated with a time step of 0.4 ms, and was numerically integrated by Euler methods using Matlab software (R2021a, Mathworks, USA). During encoding phase, the recurrent and PP synaptic weights were modified under the STDP rules. The dependence of LTP level on the spike timing difference between pre and post-synaptic cells ($\Delta t = t_{post} - t_{pre}$) is shown in Fig. S7Ba-Bb.

Assumptions for the CA3 network model. We consider an animal, which experience a series of episodes. We call MF and PP afferent inputs to CA3-PCs carrying the information of *i*-th episode as *i*-th pattern ($\boldsymbol{P}_i$).

1. *MF inputs are strong and sparse, while PP inputs are weak and diffuse*: Only a small and non-overlapping subset of CA3-PCs receive MF input during encoding (or learning) phase, while almost all CA3-PCs receive PP inputs with different strength. Henceforth, a group of CA3-PCs that receive MF inputs carrying information of the *i*-th pattern ($\boldsymbol{P}_i$) will be denoted as $\mathbf{M}_i$ subset.
2. *Distributions of MF and PP input strength are skewed*: During encoding phase, the MF input strength to CA3-PCs of a given **M** subset follows a log-normal distribution (Buzsaki & Mizuseki, 2014). We assumed that a small fraction of CA3-PCs in a given **M** subset receive strong MF inputs, in which LTP-

263 IE is induced by concerted actions of intracellular Ca^{2+} and Zn^{2+} signaling (Eom et al., 2019). A subset of
264 CA3-PCs that underwent LTP-IE during encoding of $\boldsymbol{P}_i$ will be denoted as $\mathbf{M}_i$*.

265 3. *LTP at A/C and PP synapses requires converging MF inputs*: Because A/C and PP synapses display
266 Hebbian plasticity (McMahon & Barrionuevo, 2002; Mishra et al., 2016; Tsukamoto et al., 2003)), LTP
267 at A/C and PP synapses is critically dependent on the postsynaptic firing. Sparse and strong MF input
268 provides an additional variance in the excitatory input distribution over the CA3-PC population and
269 thus governs the firing pattern of CA3-PCs during a learning phase under competitive *k*-Winners-Take-
270 All regime (O'Reilly & McClelland, 1994; Treves & Rolls, 1992). Moreover, acetylcholine (Ach) level is
271 high during encoding phase, and the high Ach reduces the A/C synaptic strength by 50% (Hasselmo,
272 2006; Vogt & Regehr, 2001). As a result, LTP at A/C and PP synapses is supervised by MF inputs that
273 carry information of an episode. The memory for *i*-th episode ($\boldsymbol{E}_i$) is stored at PP and A/C synapses of
274 CA3-PCs comprising $\mathbf{M}_i$ subset (referred to as $\mathbf{M}_i$ PCs).

275 **Data analysis.** Electrophysiological data were acquired and digitized using an analogue-to-digital
276 converter (Digidata 1440A, Molecular Devices) and stored in a computer hard disk. Analyses of data were
277 performed with Igor Pro (version 6.10A; WaveMetrics, Lake Oswego, OR, USA) and Clampfit 10.2
278 (Molecular Devices, Sunnyvale, CA, USA). We used the bias-corrected version of Akaike information
279 criterion (AIC) to select a better distribution model for the histogram data of fluorescence intensities in
280 Fig. S4D (Hurvich & Tsai, 1989). Statistical data are expressed as mean ± standard error of the mean (SEM),
281 and the number of cells measured (denoted as *n*). Statistical data were evaluated for normality and
282 variance equality with Kolmogorov-Smirnov test and Levene's test, respectively. For data that satisfy
283 normality and equality of variances, statistical evaluations were performed with Student's t-test or
284 general linear model (GLM). For data that did not satisfied above properties, nonparametric tests, such as
285 Mann-Whitney U test or Wilcoxon signed rank test, were performed to evaluation. For simplicity of
286 description, significance level (P) was marked as $P < 0.05$. n.s., no statistical significance; $^{*}P < 0.05$; $^{**}P <$
287 0.01; $^{***}P < 0.005$ in figures. Statistics processing was performed with PASW Statistics 18 (SPSS Inc, 2009,
288 Chicago, IL, USA).

289

290 ## Results

291 ### *1. Differential effects of intracellular glutathione on somatic and MF-induced LTP-IE*

292 The LTP-IE is mediated by Ca^{2+} and protein tyrosine kinase (PTK)-dependent downregulation of Kv1.2,
293 which is antagonized by receptor protein tyrosine phosphatase alpha (RPTPα) (Fig. S1) (Eom et al., 2019).
294 RPTPα is activated by PKC, and inactivated by oxidative stress and Zn^{2+} (Blanchetot et al., 2002; Meng et
295 al., 2002). Reducing molecules such as reduced form of glutathione (GSH) are normally present in cytosol
296 in millimolar range (Forman et al., 2009). Intracellular perfusion with the conventional whole-cell patch
297 pipette solution lacking reducing molecules may bias the cellular redox to oxidized state. To prevent
298 inactivation of protein tyrosine phosphatase (PTP) during whole-cell recording (WCR), we added 5 mM
299 GSH to the pipette solution. We confirmed that input conductance (G_{in}), PP-evoked EPSPs (PP-EPSPs) and
300 action potential (AP) parameters were stable up to 45 min of WCR in the presence of 5 mM GSH (Fig. S2).
301 Henceforth, all the whole-cell patch experiments shown in Fig. 1-4 were done using pipette solution
302 containing GSH, unless stated otherwise.
303 The long lasting increases in input resistance (inverse of G_{in}) and PP-EPSPs are the hallmarks of LTP-IE in
304 CA3-PCs, which can be induced by 10 Hz somatic AP firing (somatic conditioning, SC) or 20 Hz MF
305 stimulation (MF conditioning)(Eom et al., 2019; Hyun et al., 2015; Hyun et al., 2013). After measuring the
306 baseline G_{in} for 5 min, the somatic or MF conditioning was delivered (black or red arrowhead, respectively).
307 To our surprise, in the presence of GSH, the SC-induced decrease in G_{in} was not sustained (Fig. 1Aa-c),
308 whereas it was without GSH (Hyun et al., 2013). This GSH effect was not observed after MF conditioning.
309 The acceleration of the 1st AP latency measured from voltage responses to a ramp current (250 pA/s) was
310 in parallel with those of G_{in} (Fig. 1Ad-Ag). Both somatic and MF conditioning increased PP-EPSPs, but faster
311 as previously observed (Hyun et al., 2015) (Fig. 1Ba-Bc). As expected, the SC-induced increase in PP-EPSP
312 was not sustained, whereas those after MF conditioning stayed enhanced (Fig. 1Ba-Bc). Neither somatic
313 nor MF conditioning altered the amplitude of PP-EPSCs (Fig. 1Bd-Be). EPSC amplitude depends on
314 neurotransmitter release and AMPA receptor expression but little on intrinsic excitability. Thus, these
315 results suggest that MF inputs augment CA3 dendritic excitability thereby increasing PP-EPSPs. Given that
316 PTP activity is preserved by GSH in the pipette solution, our results suggest that PTP may rapidly reverse
317 the LTP-IE induced by SC but not that by MF conditioning. This results can be understood in light of our
318 previous findings that MF conditioning induces not only Ca^{2+} but also Zn^{2+} signaling, and the latter
319 facilitates LTP-IE by reversible inhibition of PTP (Eom et al., 2019). Somatic conditioning which induces

320 Ca^{2+} transients (CaTs) without Zn^{2+} signaling, however, may activate both PTKs and PTPs (Brandt et al.,
321 2003; Eom et al., 2019; Lev et al., 1995; Tsai et al., 1998), and lead to the short-lasting potentiation of
322 intrinsic excitability (PIE). This result is in stark contrast to our previous observation that SC readily induced
323 long-lasting PIE in the absence of GSH (Hyun et al., 2013).
324

325 *2. Depotentiation of MF-induced potentiation of PP-fEPSPs by A/C synaptic stimulation*

326 We hypothesized that CaTs without Zn^{2+} signaling may reverse MF-induced LTP-IE when the activity of
327 PTP is preserved. CaTs without Zn^{2+} signaling can be evoked by stimulation of soma or afferent fibers other
328 than MFs (non-MF) such as PP or associational/commissural (A/C) fibers (Eom et al., 2019). To prevent
329 perturbation of the intracellular milieu of CA3-PCs, we monitored PP-evoked field EPSPs (PP-fEPSPs)
330 before and after MF conditioning and subsequent A/C fiber stimulations. The recording and stimulating
331 electrodes were placed as shown in Fig. 2Aa (see Materials and Methods). Stimulation of PP evoked a
332 negatively deflecting fEPSP at the recording electrode placed in stratum lacunosum-moleculare (SLM)
333 (gray-black, Fig. 2Ab), while stimulation of MFs (cyan) and A/C fibers (red) evoked positive fEPSP at SLM.
334 To evoke antidromic firing of CA3-PCs and activate A/C synapses, the alveus of CA3 was stimulated with
335 40 pulses for 2 s, which induced AP bursts following EPSP summation in the CA3-PC under WCR (Fig. 2B).
336 Both EPSPs and AP bursts were abolished by bath application of CNQX, suggesting that antidromic firings
337 of CA3-PCs activated A/C inputs to the CA3-PC under WCR, resulting in AP bursts.
338 We regarded the maximal slope over an initial half of rising phase of fEPSP as an initial slope of PP-fEPSP.
339 The initial slope of fEPSP represents fast EPSC, while the peak fEPSP amplitude reflects delayed activation
340 of somato-dendritic currents as well as synaptic current (Garcia et al., 2010). Fig. 2Ca-b shows the input-
341 output relationships for the peak amplitude and initial slope of PP-fEPSP, respectively. The latency of PP-
342 fEPSPs was not altered by the increase in stimulation intensity (Fig. 2Cc). The PP-fEPSPs were attenuated
343 by bath application of DCG-IV, an agonist of group II mGluR, which is highly expressed in PP (Shigemoto
344 et al., 1997)(Fig. 2Cd).

345 MF conditioning enhanced the peak amplitude of PP-fEPSP, but not the initial slope of PP-fEPSPs (Fig. 2Da
346 and 2Ea), consistent with our patch clamp findings that MF conditioning enhanced PP-EPSPs, but not PP-
347 EPSCs (Fig. 1). Indeed, the alveus stimulation (10 pulses at 50 Hz, A/C conditioning) applied at 20 min after
348 MF conditioning induced gradual decrease in the peak amplitude of PP-fEPSPs (Fig. 2D). The initial slope
349 of PP-fEPSPs and paired pulse ratio (PPR) of slopes were not affected by MF and A/C conditioning (Fig. 2E),

350 suggesting that changes in dendritic excitability of CA3-PCs underlie the MF-induced potentiation and A/C-
351 induced depotentiation of PP-fEPSPs.

352

353 *3. MF-induced LTP-IE is de-potentiated by somatic or A/C synaptic stimulation, and is hindered*
354 *by Zn^{2+}*

355 To test whether the results of field recordings can be replicated in whole-cell recordings, we examined
356 the effects of alveus stimulation on MF-induced LTP-IE. The MF conditioning decreased the G_{in} of CA3-PCs
357 (73.5 ± 1.8%, n = 21, Fig. 3Aa-Ad). The G_{in} of CA3-PCs was restored to the baseline by a train of stimuli (10
358 pulses at 20 Hz) delivered to the alveus at 15 min after MF conditioning (Fig. 3Aa), consistent with the
359 results of field recordings (Fig. 2). To avoid inadvertent recruitment of various neuromodulator pathways
360 by alveus stimulation, we tested whether direct somatic stimulation can depotentiate MF-induced LTP-IE.
361 Somatic AP bursts comprised of 10 spikes at 100 Hz, a typical burst firings of CA3-PCs in vivo (Kowalski et
362 al., 2016), applied at 15 min after MF conditioning also restored the G_{in} to the baseline (Fig. 3Ab). To assess
363 the minimal somatic stimulation required for depotentiation, we examined the effects of somatic
364 stimulation with fewer number of spikes. Surprisingly, the bursts of two APs at 100 Hz restored G_{in} to the
365 baseline level (Fig. 3Ac). We examined depotentiation of PP-EPSPs too. Similar to the G_{in} changes, MF-
366 induced potentiation of PP-EPSPs (197.5 ± 19.9%, n = 21, Fig. 3Ba-Bd) was reversed by AP bursts elicited
367 by alveus stimulation (Fig. 3Ba) or by direct injection of ten (Fig. 3Bb) or two (Fig. 3Bc) supra-threshold
368 somatic current pulses at 100 Hz. The amplitudes of PP-EPSCs were not altered after MF conditioning or
369 depotentiation stimulation (time, $F_{(2,18)} = 0.017$, $p = 0.897$; stimuli, $F_{(2,18)} = 0.718$, $p = 0.501$; stimuli × time,
370 $F_{(2,18)} = 0.299$, $p = 0.745$; GLM and simple effect analysis). The changes of G_{in} and PP-EPSPs before and
371 after MF conditioning and depotentiation stimulation are summarized in Fig. 3Ad and Bd, respectively.
372 Somatic AP bursts did not depotentiate MF-induced LTP-IE in the presence of 100 nM $ZnCl_2$, which was
373 added to aCSF 10 min after MF conditioning (Fig. 3C), indicating that lack of Zn^{2+} signaling during AP bursts
374 is essential for depotentiation. This result supports our hypothesis that CaTs without Zn^{2+} signaling
375 activates PTP and triggers depotentiation of LTP-IE.

376

377 *4. MF-induced LTP-IE is reversed by homosynaptic induction of LTP at PP-CA3 synapses*

378 MF-induced LTP-IE heterosynaptically potentiates PP-EPSPs, but not PP-EPSCs, because LTP-IE enhances
379 dendritic excitability with little effect on synaptic transmission *per se*. We will refer to homosynaptic LTP

380 of PP-EPSCs as PP-LTP, distinct from MF-induced hetero-synaptic LTP of PP-EPSPs accompanied with LTP-
381 IE. Previously we showed that LTP-IE lowers the threshold for PP-LTP in the mice hippocampal CA3 (Eom
382 et al., 2022). We confirmed this notion in the rat CA3 (Fig. S3 and Supplementary Results).

383 Above results suggest that MF-induced LTP-IE can be reversed by somatic burst firings elicited by somatic
384 or A/C stimulation (Fig. 2-3), and that MF-induced LTP-IE enables weak PP inputs to elicit APs and induce
385 Hebbian PP-LTP (Fig. S3). We posed a question whether AP firing elicited by weak PP inputs in a MF-
386 conditioned CA3-PC can reverse LTP-IE in the presence of GSH. To this end, we simultaneously monitored
387 PP-EPSPs (Fig. 4Aa) and G_{in} (Fig. 4Ba), while MF conditioning and subsequently weak high-frequency
388 stimulation of PP (PP-HFS) were delivered to induce LTP-IE and PP-LTP, respectively. MF conditioning (Fig.
389 4Ab) enhanced PP-EPSPs but not PP-EPSCs (Fig. 4Aa), and decreased G_{in} (Fig. 4Ba). At 5 min after MF
390 conditioning, we delivered PP-HFS, which readily evoked AP firings (Fig. 4Ac) unlike naïve CA3-PCs (Fig.
391 S3Aa). After PP-HFS, both the PP-EPSPs (*left*) and PP-EPSCs (*right*) were increased (Fig. 4Ca). However, the
392 G_{in} that had been reduced by MF conditioning was restored to the baseline level (Fig. 4B). The EPSP/EPSC
393 ratio that had been increased by MF conditioning returned to the baseline after PP-HFS as shown in Fig.
394 4Cb. These results indicate that high-frequency MF inputs prime CA3-PCs for PP-LTP expression by
395 lowering the LTP threshold so that subsequently incoming high-frequency PP inputs readily elicit AP bursts
396 in the primed PCs, and that the PP-induced AP bursts lead to both PP-LTP induction and termination of
397 MF-induced LTP-IE.

398

399 *5. LTP-IE occurs in hippocampal CA3 region, and lasts less than 3 hours in vivo*

400 We examined whether LTP-IE occurs in CA3 ensemble cells activated when rats are exposed to a novel
401 context. We labeled an ensemble of CA3-PCs activated by contextual fear conditioning (CFC) using AAV-
402 RAM-d2tTA-TRE-EGFP (Sorensen et al., 2016). Rats were kept on doxycycline-free diet for 2 days before
403 being subject to CFC. Just after CFC, rats were injected with doxycycline (10mg/kg of body weight), and
404 kept in their home-cage for 1, 1.5 or 3 hours before *ex vivo* examination of G_{in} in CA3-PCs (Fig. 5Aa). At
405 about 30 min WCR of EGFP(+) CA3-PCs, we could observe the diffusion of EGFP into the patch pipette (Fig.
406 5Ab-d). Fig. 5B shows the baseline G_{in} as a function of EGFP fluorescence intensity. Most EGFP(-) cells (40
407 out of 45 cells) showed high baseline G_{in} [denoted as EGFP(-/high), black symbols], but a few of them (5
408 cells) showed low G_{in} [EGFP(-/low), yellow symbols]. The average baseline G_{in} of EGFP(+) CA3-PCs at 1 hour
409 [red symbols, denoted as EGFP(+/1hr) cells] and at 1.5 hours [blue symbols, EGFP(+/1.5hr) cells] were

410 significantly lower than those of EGFP(-/high) cells, and not different from G_{in} of GFP(-/low) cells. On the
411 other hand, G_{in} of EGFP(+) cells at 3 hours [green symbols, GFP(+/3hr) cells] were not different from those
412 of GFP(-/high) cells. Therefore, cells were categorized into high and low G_{in} cell groups: GFP(-/high) and
413 GFP(+/3hr) cells *vs*. GFP(-/low), GFP(+/1hr) and GFP(+/1.5hr) cells under the significance level of 0.05
414 [$F_{(4,,72)} = 38.667$, $p < 0.001$, Tukey HSD]. Since most ensemble cells displayed lower G_{in}, the GFP(-/low) cells
415 may represent CA3 ensemble cells that are not infected by AAV.

416 The inducibility of LTP-IE was evaluated by comparing G_{in} at 30 min after somatic conditioning (denoted
417 as post-SC G_{in}) with baseline values. in the low G_{in} cell group, SC did not induce additional decrease of G_{in}
418 (Fig. 5C), while LTP-IE was readily induced in the high G_{in} cell group [baseline vs. post-SC, $p < 0.001$ in
419 GFP(-);$p < 0.554$ in GFP(+/3hr); GLM and simple effect analysis]. Moreover, the post-SC G_{in} values were
420 not different among all groups (baseline, $F_{(3,24)} = 14.616$, $p < 0.001$; post-SC, $F_{(3,24)} = 0.706$, $p = 0.558$, GLM
421 and univariate analysis), suggesting that GFP(-/low), GFP(+/1hr) and GFP(+/1.5hr) cells may have already
422 undergone LTP-IE. The similarity of GFP(+/3hr) to the GFP(-/high) cells indicates that LTP-IE of CA3-PCs
423 does not last longer than 3 hours *in vivo*, and implies that there may be a mechanism that reverses the
424 increased intrinsic excitability while the animal is kept in their homecage (see Discussion).

425

426 *6. LTP-IE occurs in CA3 ensemble cells and is reversed in a subset of putative twice-activated*
427 *ensemble cells*

428 Given that the LTP-IE of CA3-PCs is maintained at least for 90 min after CFC, we wondered whether the
429 LTP-IE can be reversed earlier by formation of an additional ensemble in the CA3 area. To ensure labeling
430 of all ensemble cells, we further studied the excitability of ensemble cells using B6.Cg-Tg(Fos-tTA,Fos-
431 EGFP*)1Mmay/J mice (referred to as cfos-shEGFP mice), which express short half-life green fluorescent
432 protein (shEGFP, $t_{1/2}$ = 2 hours) under the control of c-*fos* promoter. We compared the fluorescence
433 intensity distribution of CA3 shEGFP(+) cells in cfos-shEGFP mice exposed only once to a context A (ctxA
434 mice) with that in mice exposed to two contexts (A and B; ctxAB mice) sequentially with a 30 min time
435 interval, and found that the latter mice harbor shEGFP(+) cells with distinctly higher fluorescence intensity
436 (Fig. S4 and Supplemental Results).

437 We examined whether the input resistance of CA3-PCs has any correlation with their epi-fluorescence
438 intensity *ex vivo* from ctxA and ctxAB mice (Fig. 6Aa). For ctxA mice, excitability was examined at two time
439 points: at 60 and 90 min after being kept in their home cage (Fig. 6Aa; ctxA60 and ctx90 mice, respectively).

440 As shown below, shEGFP(+) CA3-PCs in ctxA60 and ctx90 mice [denoted as ctxA60(+) and ctxA90(+) cells,
441 respectively] were not different in fluorescence intensity and excitability parameters. To correct the
442 depth-dependent fluorescence attenuation in epifluorescence microscopy, we added 50 µM Alexa Flour
443 594 (AF594; Invitrogen) to a patch pipette solution for ratio-metric measurement of shEGFP and AF594
444 fluorescence intensities. Consistent with the results of Fig. S4, a subset of shEGFP(+) CA3-PCs from the
445 ctxAB mice displayed higher green-to-red fluorescence (G/R) ratio than the maximal G/R ratio of ctxA60(+)
446 or ctxA90(+) cells, and will be referred to as ctxAB(++) cell (Fig. 6Bc-d). The other subset which had G/R
447 ratio similar to ctxA60(+) and ctx90(+) cells, and will be referred to as ctxAB(+) cell (Fig. 6Ba-b). The G/R
448 ratios of all shEGFP(+) cells could be categorized into two groups: a group comprised of ctxA60(+),
449 ctxA90(+) and ctxAB(+) cells and the other group of ctxAB(++) cells [$F_{(3,43)} = 39.741$, $p < 0.001$, ANOVA and
450 Tukey HSD, Fig. 6Be]. Because ctxAB(++) cells were observed only in the mice which visited context A and
451 B, the high G/R ratio of ctxAB(++) cells may be caused by double activation of c-*fos* promoter in the
452 contexts A and B.

453 The baseline G_{in} values for ctxA60(+) and ctxA90(+) cells were significantly lower than those of GFP(-) cells
454 ($p < 0.001$ for both), and were not further decreased by SC (ctxA60(+), $p = 0.814$; ctxA90, $p = 0.126$),
455 suggesting that these cells have already undergone LTP-IE while the animal visited context A. The baseline
456 G_{in} and LTP-IE inducibility of ctxAB(+) CA3-PCs were similar to those of ctxA60(+) or ctxA90(+) cells [For
457 baseline G_{in}, $p = 0.819$; For pre- vs post-SC G_{in} of ctxAB(+) cells, $p = 0.873$; Fig. 6Cd-Cf]. In contrast, the
458 excitability of ctxAB(++) CA3-PCs was heterogenous. To test the inducibility of LTP-IE for ctxAB(++) cells,
459 the ratio of post-SC G_{in} over baseline G_{in} was measured. The ctxAB(++) cells were plotted on the plane of
460 the G_{in} ratio *vs.* baseline G_{in}, and were clustered using *k*-means algorithm, yielding two clusters shown in
461 Fig. 6Cc. The low and high baseline G_{in} groups are referred to as ctxAB(++/1) cells ($n = 11$) and ctxAB(++/2)
462 cells ($n = 9$), respectively (Baseline G_{in}, $t = 4.775$, $p < 0.001$; G_{in} ratio, $t = -8.115$, $p < 0.001$). The baseline
463 G_{in} and the G_{in} ratio are shown as a function of G/R ratio in Fig. 6Cd and in Fig. 6Ce, respectively. Both
464 baseline G_{in} and G_{in} ratio of shEGFP(+) cells were categorized into two groups: GFP(-) and ctxAB(++/2) *vs*.
465 ctxA60(+), ctxA90(+), ctxAB(+) and ctxAB(++/1), which will be referred to as low and high excitability
466 groups, respectively [For baseline G_{in}, $F_{(5,32)} = 12.883$, $p < 0.001$; For G_{in} ratio, $F_{(5,32)} = 19.565$, $p < 0.001$;
467 ANOVA and Tukey HSD]. The mean G_{in} values before and after SC are summarized in Fig. 6Cf. The baseline
468 G_{in} values within high excitability groups were not different one another, but significantly lower than the
469 baseline G_{in} of GFP(-) cells [baseline G_{in} (gray bars), $F_{(5,31)} = 13.053$, $p < 0.001$; post-SC G_{in} (red bars), $F_{(5,31)}$

470 = 1.213, p = 0.364, Univariate analysis], and rather similar to the post-SC G_{in} of GFP(-) cells (χ^2 = 7.279, df
471 = 3, p = 0.064, Kruskal-Wallis test).

472 The 1st AP latency and PP-EPSP/EPSC ratio reflect the excitability of soma and distal apical dendrite,
473 respectively. Comparing these parameters in different cell groups, we found that both of them are highly
474 correlated with the baseline G_{in}: faster 1st AP latency and high EPSP/EPSC ratio in high excitability cell
475 group and vice versa (Fig. S5 and S6, respectively; see Supplemental Results). These results suggest that
476 CA3 ensemble cells except ctxAB(++/2) cells had already underwent LTP-IE *in vivo*. In contrast, ctxAB(++/2)
477 cells were not different from GFP(-) cells with regard to all aspects: baseline G_{in}, the 1st AP latency, and
478 EPSP/EPSC ratio, and their pre- vs post-SC ratios (Fig. 6Cc, S5Ba and S6E), suggesting that ctxAB(++/2) cells
479 are not different from GFP(-) cells in somatic and distal dendritic excitability, even though they are
480 supposed to be recruited to ensembles A and B twice. We discussed below possible mechanisms
481 underlying the heterogeneity of ctxAB(++) cells (see Discussion).

482

483 *7. Lack of LTP-IE in the ensemble CA3-PCs of ZnT3 hetero-knockout mice*

484 The results of the present study together with Eom et al. (2019) indicate that MF-induced Zn^{2+} signalling
485 inhibits PTP, and thus widens the cytosolic [Ca^{2+}] window for LTP-IE induction and maintains LTP-IE in the
486 normal redox state. We tested whether LTP-IE occurs *in vivo* when MF-induced Zn^{2+} signalling is disrupted
487 by hetero-insufficiency of ZnT3, a vesicular Zn^{2+} transporter. To this end, ZnT3 hetero-knockout(HT) x cfos-
488 shEGFP hybrid mice (ZnT3HT/cfos-EGFP) were made by crossing ZnT3-knockout (KO) mice with cfos-
489 shEGFP mice. We confirmed that LTP-IE was induced by 20 Hz MF stimulation but not by 50 Hz stimulation
490 in CA3-PCs of ZnT3HT mice (n =5, t = -1.141, p = 0.318, paired t-test; Fig. 7A), similar to those of ZnT3-KO
491 mice (Eom et al, 2019). Next, we examined correlation of G_{in} with G/R ratio in ZnT3HT/cfos-shEGFP mice
492 which experienced context A and B (Fig. 7B). Unlike wildtype CA3-PCs, CA3-PCs of ZnT3HT/cfos-shEGFP
493 mice exhibited high G_{in} regardless G/R ratio (Fig. 7C and Da). Moreover, 10 Hz somatic conditioning
494 induced LTP-IE in high G/R ratio cells as well as GFP(-) cells (Fig. 7C and Db), indicating that induction
495 and/or maintenance of LTP-IE are impaired in vivo in ZnT3-HT mice. Given that dendritic Zn^{2+} transients in
496 CA3-PCs were induced by MF inputs but not by PP or A/C inputs, these results suggest that CA3-PCs that
497 received high-frequency MF inputs undergo LTP-IE in vivo.

498

499 *8. Computational modelling of the association of two sequential events in the CA3 network*

500 Our results suggest that high-frequency MF inputs prime a CA3-PC, and high-frequency PP inputs to a
501 primed CA3-PC not only induce homosynaptic LTP and but also reverse the prior MF input-induced LTP-IE
502 (Fig. 4). To conceive possible roles of this learning rule in the CA3 network dynamics, we incorporated it
503 into a CA3 recurrent network model. The assumptions adopted for the network model is based on the
504 Hebb-Marr network (McNaughton & Morris, 1987) and the computational theory of CA3 function (Lee &
505 Kesner, 2004; Treves & Rolls, 1992), and are described in detail in *Materials and Methods*.

506 To implement the LTP-IE-based learning rules, we constructed a computational model of recurrent
507 network comprised of 1000 PCs and 200 interneurons (INs) *in silico*, which are numbered with indices
508 from 1 to 1000 and 1001 and 1200, respectively. Fig. 8A and Fig. S7A show the schematic synaptic
509 connections between PCs and INs, and the initial connectivity map of the model network, respectively.
510 We assumed that PCs make excitatory synapses with each other with the probability of 10%. The synaptic
511 weights between PCs were randomly set to a value between 0 and 0.35 nS. The spike properties of PCs
512 and INs were assumed to follow a leaky integrate and fire model using parameter sets as described in
513 Materials and Methods.

514 We considered an animal which experiences a series of episodes. During each episode, MF and PP
515 afferent inputs are assumed to present the information of *i*-th episode as *i*-th input pattern (denoted as
516 $\boldsymbol{P}_i$) to CA3-PCs. The model network was trained by four patterns that arrive at the network in a sequence
517 with different time intervals (0.8-1.2 s) as shown in Fig. 8Ba (We adopted here short time intervals to
518 lessen computational time, but longer time intervals do not alter the main conclusion). Each input pattern
519 is comprised of sparse non-overlapping MF and diffuse PP inputs (red and blue dots in Fig. 8Ba,
520 respectively). The arrival of MF inputs in each pattern is confined in a subset of 200 PCs, which constitute
521 an **M** subset, while PP inputs arrive over all the PCs in the network. We assumed that each PC receives
522 different numbers of MF or PP inputs per a pattern, which are randomly given under a log-normal
523 distribution (Ikegaya et al., 2013) (Fig. 8Ba and Fig. S7D). During the encoding phase, PP and A/C synapses
524 of PCs undergo plastic changes under the spike timing dependent plasticity (STDP) rules. We assumed
525 symmetric and asymmetric STDP curves for A/C and PP synapses, respectively (Mishra et al., 2016) (Fig.
526 S7B).

527 Our results suggest that coincident increases in cytosolic [Ca^{2+}] and [Zn^{2+}] induce LTP-IE, while [Ca^{2+}]
528 increase alone reverses LTP-IE. In our simulation, the [Ca^{2+}] and [Zn^{2+}] thresholds required for triggering

529 LTP-IE were set such that MF input-induced Ca^{2+} and Zn^{2+} transients cross the threshold in about 25% of
530 PCs of an **M** subset during encoding phase. A subset of CA3-PCs that undergo LTP-IE during encoding of $\boldsymbol{P_i}$
531 will be denoted as $\mathbf{M_i}$*****. Exemplar traces for $[Ca^{2+}]_i$ and $[Zn^{2+}]_i$ simulated in an $\mathbf{M_1}$***** PC are shown in Fig. 8C.
532 To simulate the time course of excitability change we defined an intrinsic excitability parameter, *IE*, which
533 varies from 0 to 1. *IE* is equal to 0 when a cell is in a resting state, and it starts to increase toward one
534 when both $[Ca^{2+}]_i$ and $[Zn^{2+}]_i$ co-incidentally surpass the Ca^{2+} and Zn^{2+} thresholds (Caθ1 and Znθ,
535 respectively). Once *IE* is increased by MF inputs, it stays high until a CaT that surpasses another Ca^{2+}
536 threshold (Caθ2) occurs devoid of a ZnT. PP inputs to such PCs with high *IE* can readily induce APs
537 independent of MF inputs. To simulate this, a transient current was injected upon arrival of PP inputs to
538 a primed PC that has *IE* > 0.7 (Fig. S7C)(Jahnke et al., 2015). The PP input to a primed cell readily elicits
539 APs in a postsynaptic PC resulting in a CaT devoid of Zn^{2+} signaling. When the peak of a PP-induced CaT is
540 higher than a given Ca^{2+} threshold (Caθ2), the *IE* returns to zero (de-potentiation; Fig. 8C). Fig. 8Bb shows
541 the simulation results for the firing of PCs in response to the four sequentially incoming input patterns
542 shown in Fig. 8Ba. The PP inputs of $\boldsymbol{P_2}$ readily elicit firings of the $\mathbf{M_1}$***** PCs (subset of primed PCs in $\mathbf{M}_1$), and
543 thus fire together with PCs of the $\mathbf{M_2}$ subset. These concomitant firing of PCs in $\mathbf{M_1}$***** and $\mathbf{M_2}$ subsets allows
544 recurrent synapses to be strengthened between the two orthogonal ensembles. Fig. 8D shows a matrix of
545 recurrent synaptic weights consequent to these auto- and hetero-associative learning rules.
546 Next, we tested whether the recurrent network trained under these learning rules recalls the whole
547 sequence of memories from a partial cue of $\boldsymbol{P}_1$. We assumed no reduction in A/C synaptic weight during
548 recall, because recall occurs under the low cholinergic state. To trigger pattern completion-based recall
549 of the memory of $\boldsymbol{P}_1$, which is represented by $\mathbf{M_1}$, a burst of PP inputs carrying a part of $\boldsymbol{P_1}$ (denoted as $\boldsymbol{p_1}$)
550 was applied to the network (Fig. S7D). The synaptic weights of the PP inputs of $\boldsymbol{p_1}$ have been already
551 strengthened during encoding phase only in $\mathbf{M_1}$ PCs. The PP inputs of $\boldsymbol{p_1}$ drive firing in a few $\mathbf{M_1}$ PCs (14
552 PCs in the example shown in Fig. 8E), which propagated through already strengthened recurrent
553 connections, resulting in pattern completion-based recall of $\mathbf{M_1}$ (Fig. 8E). Meanwhile, the activation of PCs
554 in $\mathbf{M_1}$* plays a role of partial cue to $\mathbf{M_2}$, and triggers the second pattern completion-based recall of $\mathbf{M_2}$. In
555 this way, the PP inputs carrying a partial cue of $\boldsymbol{P}_1$ trigger the recall of whole sequence of memories that
556 were hetero-associated during encoding phase (from $\mathbf{M_1}$ to $\mathbf{M_4}$). This simulation implies that LTP-IE may
557 allow the CA3 network to recall of memories of sequential events, even if they are temporally
558 discontiguous. The simulation results are summarized in Supplemental Results.

559

560 ## Discussion

561 ### *LTP-IE may occur in the CA3 ensemble cells*

562 The present study suggests that LTP-IE is de-potentiated not only by PP inputs probably during the
563 encoding phase (Fig. 4) but also without any episodic events within 3 hours (Fig. 5). A/C input strength is
564 critically modulated by acetylcholine (Ach) level. High Ach level in the hippocampus during awake and
565 active learning state enhances MF synapses and suppresses A/C synapses (Vogt & Regehr, 2001). When
566 Ach level is low during a retrieval or consummatory phase, the suppression of A/C synapses is relieved
567 resulting in spontaneous offline reactivation of neuronal ensembles, manifested as sharp wave ripples
568 (SWRs). Unlike PP-EPSPs, A/C-EPSPs are not enhanced by LTP-IE (Hyun et al., 2015). In the low cholinergic
569 state, however, A/C input-driven firings of CA3-PCs would be facilitated (Kowalski et al., 2016; Malezieux
570 et al., 2020), and may contribute to depotentiation of LTP-IE even if A/C inputs do not induce IEG
571 activation. This possibility may be responsible for depotentiation of LTP-IE while animals were kept in the
572 homecage. It remains to be tested whether the A/C synaptic inputs to CA3-PCs during low cholinergic
573 state contribute to de-potentiation of LTP-IE.

574 Immediate early gene (IEG)-induced expression of fluorescence protein has been widely used for labeling
575 neuronal ensembles to investigate the recall of memory represented by the labeled ensemble. To
576 investigate whether LTP-IE is reversed by the second activation of ensemble cells, it is essential to
577 distinguish once- *vs*. twice-activated ensemble cells in an animal that experienced two contexts within 2
578 hours because LTP-IE is spontaneously reversed less than 3 hours (Fig. 5). No currently available labeling
579 technique meets these requirements, although techniques for labeling active population of neurons with
580 high temporal precision has been recently developed (Lee et al., 2017; Moeyaert et al., 2018). Thus, we
581 compared the expression of c-fos promoter-induced shEGFP expression level between cfos-shEGFP
582 transgenic mice which were exposed a novel context once and twice (denoted as ctxA and ctxAB mice).
583 Because a subset of ensemble CA3-PCs from the ctxAB mice expressed distinctly high level of shEGFP
584 compared to those from the ctxA mice observed by both confocal and epifluorescence microscopy (Fig.
585 S4 and Fig. 6), we regarded such shEGFP(++) subset as twice-activated ensemble cells. Nevertheless, it
586 cannot be ruled out that it contains once-activated ensemble cells.

587

588 *Why a subset of ctxAB(++) cells exhibit G_{in} similar to that of non-ensemble cells?*

589 CA3-PCs with distinctly high EGFP expression from ctxAB mice were comprised of mixed population in the
590 excitability (Fig. 6 and Fig. S5-S6). Why ctxAB(++/2) cells exhibit the normal excitability despite that these
591 cells may participate in both ensembles encoding contexts A and B? There are two possibilities for the
592 normal excitability of ctxAB(++/2) cells. First, these cells may have never experienced LTP-IE. Alternatively,
593 they underwent LTP-IE in context A, and the LTP-IE is de-potentiated in context B. The first possibility is
594 unlikely because most CA3 ensemble cells of the animal that visited only context A [ctxA60(+) and ctx90(+)
595 cells] exhibited high excitability. Previously we showed that MF inputs are privileged for the induction of
596 LTP-IE (Eom et al, 2019). Moreover, Figure 1 suggests that, even if the excitability would be enhanced by
597 non-MF inputs, the high excitability state cannot be sustained longer than 30 min under the physiological
598 redox conditions. This notion is supported by the ex vivo results that the CA3 ensemble cells in ZnT3-
599 heteroKO mice exhibited no sign of LTP-IE (Fig. 7). Since we examined G_{in} at 60 min after the last visit,
600 ctxAB(++) cells as well as ctxA60(+) and ctxA90(+) cells may have received high frequency MF inputs while
601 the animal visited context A, assuming that ctxAB(++) are twice-activated ensemble cells. If the latter
602 possibility is correct, the mechanism underlying de-potentiation of LTP-IE can be explained by our findings
603 that non-MF inputs can reverse the MF-induced high excitability state of CA3-PCs (Fig. 2, 3 and 4).
604 Moreover, CA3-PCs in the primed state readily fire in response to subsequently arriving high frequency
605 PP inputs, which also reverse the high excitability state (Fig. 4). Given that ctxAB(++) cells are activated
606 both in context A and B, their firing in context B can be elicited not only by MF inputs but also by PP inputs
607 alone as long as the LTP-IE is maintained while the animal visited context B. Therefore, ctxAB(++) cells may
608 be comprised of two groups: CA3-PCs that received high frequency MF inputs in both contexts, and those
609 received MF inputs in context A and subsequently only PP inputs in context B. The latter group may
610 undergo MF-induced LTP-IE in context A and PP-induced depotentiation in context B, and thus eventually
611 exhibit normal baseline G_{in}, because PP inputs can reverse the prior MF input-induced LTP-IE (Fig. 4).

612

613 *Computational implications*

614 Hippocampal CA3 has been implicated not only in non-overlapping representation of episodic memories
615 but also in the memory of sequence of temporally discontiguous events (Farovik et al., 2010). Recently,
616 the synaptic tagging and capture hypothesis and/or post-learning CREB-dependent modification of
617 intrinsic excitability have been proposed as network mechanisms that permit the overlap of ensembles

618 representing temporally separate episodes in hippocampal CA1 and amygdala (Lisman et al., 2018). This
619 overlap may be mediated by increased sharing of feedforward inputs between the ensembles because
620 recurrent connections between principal cells lack in these areas. The same regulation of ensemble
621 overlap in a recurrent network would have a detrimental effect on the orthogonality of ensembles
622 because co-active neurons tend to be strongly connected via recurrent synapses (called auto-association),
623 which may eventually lead to a merge of ensembles. Therefore, different mechanisms may be necessary
624 in order for two orthogonal ensembles to be associated (called hetero-association) in a recurrent network,
625 but it has been little understood. The LTP-IE-based hetero-association of ensembles proposed in the
626 present study prevents not only uncontrolled overlap between non-adjacent ensembles in a sequence
627 (for example, link of $\mathbf{M_1}$ and $\mathbf{M_3}$), but also further hetero-association between ensembles carrying
628 information non-adjacent events in a sequence. Therefore, the learning rule may allow two orthogonal
629 ensembles adjacent in a sequence to be linked with the overlapping fraction tightly regulated.

630

631 ## Figure Legends

632 *Fig. 1*

633 **Fig. 1 Differential effects of intracellular GSH on somatic and MF conditioning-induced LTP-IE. Aa** and
634 **Ba.** Mean baseline-normalized input conductance (G_{in}) and PP-EPSP amplitude of CA3-PCs before and
635 after MF (red) or somatic (black) conditioning (arrowheads). Right two insets of Aa, Voltage responses to
636 subthreshold current injection for measuring G_{in} before and after MF (middle) and somatic (right)
637 conditioning. Insets of Ba, PP-EPSCs (upper) and PP-EPSPs (lower) before and after MF (left) or somatic
638 (right) conditioning. The time points of recording are indicated by asterisks (same color codes). **Ab-Ac.**
639 Summary for G_{in} at baseline, 10 min and 30 min after the MF (*Ab*) or somatic (*Ac*) stimulation. For MF
640 conditioning, 0 vs. 10 min, $p < 0.001$; 0 vs. 30 min, $p < 0.001$; 10 vs. 30 min, $p = 0.190$ (GLM and simple
641 effect analysis). For somatic conditioning, 0 vs. 10 min, $p < 0.001$; 0 vs 30 min, $p = 0.533$; 10 vs. 30 min: p
642 < 0.001 (GLM and simple effect analysis). Here, the baseline values are denoted as 0. **Ad-Ae.** Voltage
643 responses to ramp current injection measured before (black), 10 min (blue) and 30 min (red) after MF (*Ad*)
644 and somatic (*Ae*) conditioning. **Af-Ag.** Mean latency of first AP before, and 10 min and 30 min after the
645 MF (*Af*) or somatic (*Ag*) conditioning (For MF, 0 vs. 10 min, $p < 0.001$; 0 vs. 30 min, $p < 0.001$; 10 vs. 30
646 min, $p = 0.964$; For somatic, 0 vs. 10 min, $p < 0.001$; 0 vs. 30 min, $p = 0.054$; 10 vs. 30 min, $p < 0.001$; GLM
647 and simple effect analysis). **Bb-Be.** Mean PP-EPSP (Bb-Bc) and PP-EPSC (Bd-Be) amplitudes at baseline, 3
648 min and 30 min after MF (Bb, Bd) or somatic (Bc, Be) conditioning. For EPSP/MF conditioning, 0 vs. 10 min,
649 $p < 0.001$; 0 vs. 30 min, $p < 0.001$; 10 vs. 30 min: $p = 0.779$. For EPSP/somatic conditioning, 0 vs. 10 min, p
650 < 0.001, 0 vs. 30 min, $p = 0.481$; 10 vs. 30 min, $p < 0.001$ (GLM and simple effect analysis).

651 *Fig. 2*

652 **Fig. 2, Restoration of MF-induced potentiation of PP-fEPSPs by A/C stimulation. Aa.** IR-DIC images for
653 extracellular recording setup. The recording electrode was placed on the CA3 SLM. Three stimulating
654 electrodes were placed on the SLM of CA1 and subiculum border, granule cell layer of dentate gyrus, and
655 alveus of CA3 to stimulated PP, MF, and A/C fibers, respectively. The silhouette of the each glass electrode
656 is indicated by a black solid line. **Ab.** Upper, Representative traces of fEPSPs evoked by paired pulse
657 stimulation of PP (PP-fEPSPs, 100 ms interval) with gradually increasing intensity ranging 10 to 70 V.
658 Middle, MF-evoked fEPSP. Lower, A/C-evoked fEPSP trace. The same color codes were used as in Aa. **Ba.**
659 IR-DIC images for whole-cell patch pipette on the CA3-PC and the glass electrode on the alveus of CA3 for
660 stimulation of A/C synapses. Yellow bars in *Aa* and *Bc*, 500 µm. **Bb.** Voltage response of the CA3-PC to A/C

661 stimulation recorded using whole-cell patch techniques before (red) and after (black) bath application of
662 CNQX. Inset, the same EPSPs evoked by first a few stimuli in an expanded scale. Scale bars, 100 ms and 10
663 mV. **Ca-Cb.** Mean peak amplitude (*Ca*) and initial slope of PP-fEPSP (*Cb*) as a function of stimulation
664 intensity. **Cc.** PP-fEPSP latency (time from PP stimulation to the peak of PP-fEPSP) was not affected by
665 stimulus intensity (linear regression slope, t = -0.02, p = 0.98, n = 5). **Cd.** Bath application of DCG-IV
666 attenuated the PP-fEPSP amplitudes (n = 5, t = 5.075, p = 0.007; paired t-test).**Da.** Peak amplitudes of 1st
667 PP-fEPSP before and after MF conditioning (blue arrowhead) and A/C conditioning (red arrowhead at 40
668 min). The PP-fEPSPs increased and reached a plateau 5 min after MF conditioning. The PP-fEPSP stayed
669 increased up to 40 min, and was restored to the baseline by A/C conditioning. **Db.** PP-fEPSP traces before
670 (black; -15 min), and after MF conditioning (blue, +40 min) and after A/C conditioning (red, +80 min).
671 Lower, the first fEPSPs in expanded time scale (gray box). The same color codes as the dots in Ca. D**c.**
672 Summary for the peak amplitudes of PP-fEPSPs before and after MF (40 min) and A/C conditioning (80
673 min) ($F_{(2,10)}$ = 17.66, p = 0.005; baseline vs. 40 min, p = 0.002; baseline vs. 80 min, p = 0.672; 40 vs. 80 min,
674 p = 0.007; n = 6, RM-ANOVA and simple effect analysis). **Ea.** Neither the initial slope of first PP-fEPSP (black;
675 $F_{(2,10)}$ = 0.174, p = 0.842) nor paired pulse ratio (PPR, light red; $F_{(2,10)}$ = 0.057, p = 0.944, RM-ANOVA and
676 simple effect analysis) measured from the peak amplitudes of 1st and 2nd PP-fEPSPs were affected by the
677 MF and A/C conditioning. **Eb.** Summary for the initial slope of PP-fEPSPs at the baseline, after MF
678 conditioning and after A/C conditioning.

679 *Fig. 3*

680 **Fig. 3 Depotentiation of MF-induced LTP-IE can be induced by somatic or A/C synaptic stimulation, and**
681 **is hindered by Zn^{2+}. Aa-Ac**. Baseline- normalized G_{in} (filled circles) changes caused by MF conditioning at
682 0 min (blue arrowhead) and by somatic AP bursts at 15 min (red arrowhead) evoked by A/C stimulation
683 (*Aa*) or direct somatic current injection of ten (*Ab*) or two (*Ac*) pulses at 100 Hz. For A/C stimulation (*Aa*),
684 0 vs. 15 min, p < 0.001; 0 vs. 30 min, p = 0.945; 15 vs. 30 min, p < 0.001 (n = 7, GLM and simple effect
685 analysis). For somatic AP bursts (*Ab*), 0 vs. 15 min, p < 0.001; 0 vs. 30 min, p = 0.936; 15 vs. 30 min, p <
686 0.001 (n = 7, GLM and simple effect analysis). For two AP simulation (*Ac*), 0 vs. 15 min, p < 0.001; 0 vs. 30
687 min, p = 0.439; 15 vs. 30 min, p < 0.001 (n = 7, GLM and simple effect analysis). The MF-induced decrease
688 of G_{in} in the absence of intracellular GSH is reproduced from (Eom et al., 2019) for comparison (*gray*
689 *symbols*). For A/C synaptic activation, CA3 alveus was stimulated at 20 Hz for 0.5 s (A/C conditioning, Aa).
690 *Left inset*, Voltage response to MF conditioning. Middle inset, AP bursts induced by A/C conditioning (Aa)
691 or somatic current injection (Ab and Ac). *Right inset*, Representative voltage responses to somatic

692 subthreshold current injection (+10 and -30 pA) for measuring G_{in} at the time indicated by black (baseline),
693 blue (at 14 min), and red (at 29 min) asterisks. The same color codes were used for the asterisks and traces.
694 **Ad.** Summary for normalized G_{in} at the baseline, 15 min after MF conditioning, 15 min after the
695 depotentiation (time: $F_{(2,18)} = 162.345$, $p < 0.001$, stimuli: $F_{(2,18)} = 1.392$, $p = 0.274$, stimuli × time: $F_{(2,18)} =$
696 1.66, $p = 0.218$; GLM and simple effect analysis). **Ba-c.** Same as Aa-Ac but peak amplitudes of PP-EPSP
697 were monitored instead of G_{in}. For alveus stimulation (*Ba*), 0 vs. 15 min: $p = 0.012$; 0 vs. 30 min, $p = 0.818$,
698 15 vs. 30 min, $p = 0.011$ ($n = 7$, GLM and simple effect analysis). For 10 somatic APs (*Bb*), 0 vs. 15 min, $p =$
699 0.012; 0 vs. 30 min, $p = 0.848$; 15 vs. 30 min, $p = 0.011$ ($n = 7$, GLM and simple effect analysis). For 2 APs
700 (*Bc*), 0 vs. 15 min, $p = 0.006$; 0 vs. 30 min, $p = 0.801$; 15 vs. 30 min, $p = 0.004$ ($n = 7$, GLM and simple effect
701 analysis). *Gray symbols*, PP-EPSP amplitudes measured without intracellular GSH, which is reproduced
702 from (Eom et al., 2019) for comparison. *Blue arrowheads*, MF conditioning at 0 min. *Read arrowheads*,
703 second conditioning by CA3 alveus stimulation (*Ba*) or somatic injection of current pulses (*Bb* and *Bc*) at
704 15 min. *Insets*, Representative traces for PP-EPSPs recorded at time points indicated by asterisks with the
705 same color codes. **Bd**. Summary for the PP-EPSP amplitudes at baseline, 15 min after MF conditioning, 15
706 min after the second conditioning (time: $F_{(2,18)} = 71.199$, $p < 0.001$, stimuli: $F_{(2,18)} = 1.392$, $p = 0.274$, stimuli
707 × time: $F_{(2,18)} = 0.822$, $p = 0.520$; GLM and simple effect analysis). **Ca.** Time course of normalized G_{in} changes
708 (filled circles) caused by MF conditioning (20 Hz for 2 s) at 0 min (blue arrowhead) and subsequent somatic
709 100 Hz AP bursts for 0.1 s at 15 min (red arrowhead). For comparison, MF-induced decrease of G_{in}
710 measured in the absence of intracellular GSH is reproduced from previous study (Eom et al., 2019) (gray
711 symbols). $ZnCl_2$ was bath-applied 10 min after MF conditioning. Note that somatic AP bursts did not trigger
712 depotentiation of MF-induced LTP-IE in the presence of 100 nM $ZnCl_2$. (15 min vs. 30 min, $p = 1.00$; simple
713 effect analysis). **Cb.** Representative voltage traces in response to subthreshold current (+10 and -30 pA)
714 for measuring G_{in}. Voltage responses were measured before and c.a. 15 min after MF conditioning, and
715 c.a. 15 min after somatic AP bursts (indicated by black, blue and red asterisks in Aa, respectively). **Cc.**
716 Summary for the mean G_{in} at baseline, 15 min after MF conditioning, and 15 min after 100 Hz AP bursts
717 ($F_{(1,4)} = 16.109$, $p = 0.016$, RM-ANOVA; 0 vs. 15 min, $p = 0.007$; 0 vs. 30 min, $p = 0.002$; 15 vs. 30 min, $p =$
718 1.00; $n = 5$, GLM and simple effect analysis).

719 *Fig. 4*

720 **Fig. 4, MF-induced LTP-IE is terminated after homosynaptic PP-LTP.** WCRs of CA3-PCs was done using
721 GSH-containing pipette solution. **Aa.** Baseline-normalized amplitudes of PP-EPSPs were increased by MF
722 conditioning (20 Hz MF stimulation for 2 s, *blue arrow*) and further by high-frequency stimulation of PP

723 (PP-HFS) with weak stimulation intensity (*red arrow*). *Insets*, Representative traces of PP-EPSPs (upper)
724 and PP-EPSCs (lower) and before (*black*), after MF conditioning (*blue*), and after PP-HFS (*red*). The
725 recording time points are indicated by numbers in the main graph. **Ab.** Representative traces for voltage
726 response to MF conditioning. **Ac.** Voltage response to weak PP-HFS (10 bursts every 10 s, 20 pulses at 100
727 Hz per a burst; baseline EPSC < 12.55 pA). Inset, gray boxed region in an expanded time scale. **Ba.** Baseline-
728 normalized G_{in} was decreased by MF conditioning (*blue arrow*) and restored by PP-HFS (*red arrow*). G_{in}
729 was monitored in the same cells as in Aa ($F_{(1,4)} = 24.064$, $p < 0.001$; RM-ANOVA). **Bb**. *Upper*, Representative
730 voltage responses to somatic current injection of +10 and -30 pA at baseline (black), after MF conditioning
731 (blue), and after PP-HFS (red). *Lower*, Mean G_{in} at baseline, 6 min after MF conditioning, and 25 min after
732 PP-HFS. Baseline vs. post-MF conditioning, $p < 0.001$; baseline vs post-PPHFS, $p = 1.00$; post-cond. vs post-
733 PPHFS, $p < 0.001$ (n = 7, GLM and simple effect analysis). **Ca.** Summary for the mean amplitudes of PP-
734 EPSPs (left, $F_{(1,4)} = 138.09$, $p < 0.001$; RM-ANOVA) and PP-EPSCs (right, $F_{(1,4)} = 35.751$, $p < 0.001$; RM-
735 ANOVA) at baseline, after MF conditioning, and after PP-HFS. For EPSP, baseline vs. post-MF cond., $p <$
736 0.001; baseline vs. post-PPHFS, $p < 0.001$; post-MF cond. vs. post-PPHFS, $p < 0.001$; (n = 7, GLM and simple
737 effect analysis). For EPSCs, baseline vs. post-MF cond., $p = 0.647$; baseline vs. post-PPHFS, $p < 0.001$; post-
738 MF cond. vs post-PPHFS, $p < 0.001$ (n = 7, GLM and simple effect analysis); **Cb.** Scatterplot for PP-EPSP vs.
739 PP-EPSC measured in the same CA3-PCs at baseline (black), after MF conditioning (blue), and after PP-HFS
740 (red). Baseline vs. post-cond., $p < 0.001$; baseline vs post-HFS, $p = 1.00$; post-cond. vs post-HFS, $p < 0.001$;
741 (n = 7, GLM and simple effect analysis).

742 *Fig. 5*

743 Fig. 5, **The LTP-IE of CA3-PC did not last longer than 3 hours in vivo. Aa.** Schematic timeline of the
744 experimental procedure. Doxycycline was administrated via intraperitoneal route to prevent further
745 expression of GFP after visiting context A. Animals were sacrificed to prepare hippocampal slices after 1
746 hr, 1.5 hrs, and 3 hrs. **Ac-Ad.** IR-DIC image (*Ab*) and fluorescence image excited at 488 nm for GFP(+) CA3-
747 PCs (*Ac*: immediately after making whole-cell configuration; *Ad*: 30 min after whole-cell configuration.
748 Note that diffusion of GFP to the whole cell pipette in *Ad*). Scalebar, 30 µm. **B.** Baseline G_{in} as a function
749 of GFP fluorescence intensity (F_{EGFP}). Most GFP(-) cells ($F_{EGFP} = 3.38 \pm 0.30$ a.u.) showed high baseline G_{in}
750 [denoted as GFP(-/high) cells]. Some of GFP(-) cells (3.97 ± 0.47 a.u.), however, showed lower baseline G_{in}
751 [denoted as GFP(-/low) cells]. GFP(+) cells after 1 hr (27.68 ± 1.11 a.u.) and 1.5 hr (28.92 ± 4.16 a.u) showed
752 lower G_{in}. In contrast, GFP(+) cells after 3 hr (25.72 ± 3.63 a.u.) showed high G_{in} similar to GFP(-/high) cells.
753 **Ca.** Time course of G_{in} before and after somatic conditioning (indicated as blue arrowhead). Time points

754 at which G_{in} was measured for comparison between cell groups and the representative traces are shown
755 in *Cb* are indicated as black and red arrowheads (before and 30 min after somatic conditioning,
756 respectively). **Cb-Cc.** Representative voltage traces for different cell groups (same color code as *B* and *Ca*).
757 Traces for baseline G_{in} [GFP(-/high), 6.25 ± 0.26 nS (n = 8); GFP(+) at 1 hr, 4.68 ± 0.33 nS (n = 8); GFP(+) at
758 1.5 hr, 4.48 ± 0.33 nS (n = 5); GFP(+) at 3 hr, 6.59 ± 0.28 nS, $p < 0.001$ (n = 7)] were indicated as gray color.
759 **Cc**, Summary of G_{in} before (gray) and after (red) somatic conditioning (time, $F_{(1,24)} = 66.042$; fluorescence,
760 $F_{(3,24)} = 3.705$, $p = 0.025$; time x fluorescence, $F_{(3,24)} = 25.712$, $p < 0.001$, RM-ANOVA; For 1 hr, baseline vs.
761 post-SC, $p = 0.837$; For 1.5 hr, baseline vs. post-SC, $p = 0.554$; GLM and simple effect analysis).

762 *Fig. 6*

763 **Fig. 6**, **LTP-IE occurs in CA3 ensemble cells and may be reversed in part of twice-activated ensemble cells**.
764 **Aa.** Timeline of experimental procedures. *Upper*: Mice were subject to CFC in context A for 5 min, and
765 kept in homecage for 1 hr or 1.5 hr before ex vivo study (ctxA60 and ctxA90 mice). **Ab**. Mice additionally
766 visited context B 25 min after CFC, and then were kept in homecage (ctxAB mice). **Ba-d.** Fluorescence
767 images of two AF594-loaded CA3-PCs with low (Ba-b) and high (Bc-d) G/R ratios. **Be.** Summary for G/R
768 ratios. **Ca.** Time course of G_{in} changes in response to somatic conditioning. Somatic conditioning (SC)
769 induced LTP-IE in GFP(-) CA3-PCs (gray symbols; n = 6, pre- vs. post-SC G_{in}, $p < 0.001$), but not other cells
770 except ctxAB(++/2) cells. *Inset*, voltage response to 10 Hz somatic conditioning for 2 s (blue arrowhead).
771 Small arrowheads indicate the time at which representative traces shown in *Cb* and *Cc* were recorded. **Cb.**
772 Representative traces for voltage responses to -30 pA and +10 pA current steps in GFP(-), ctxA60(+),
773 ctxA90(+), and ctxAB(+) cells. Traces before conditioning are depicted in gray color, and those after
774 somatic conditioning are in the same color codes as in *Ca*. **Cc.** *Upper*, Representative voltage traces for G_{in}
775 in ctxAB(++/1) and ctxAB(++/2) cells. *Lower*: ctxAB(++) cells were clustered into two groups based on
776 baseline G_{in} and G_{in} ratios before and after somatic conditioning using k-means analysis. There was a
777 significant difference between CtxAB(++/1) and CtxAB(++/2) groups, and the centroids of two cell groups
778 were depicted as cross symbols. **Cd-Ce.** Baseline G_{in} (*Cd*) and G_{in} ratio (*Ce*) as a function of green-to-red
779 fluorescence ratio (G/R ratio). The same color codes used in *Ca-Ce*.

780 *Fig. 7.*

781 **Fig. 7, LTP-IE does not occur in CA3 ensemble cells of ZnT3 hetero-knockout mice**. **Aa.** G_{in} changes before
782 and after 50 Hz MF stimulation for 1 s in CA3-PCs of ZnT3HT mice (open symbols). The G_{in} changes induced
783 by 20 Hz 2 s MF (pink) and 50 Hz 1s MF stimulation (light blue) were reproduced from our previous study

784 (Eom et al. 2019). **Ab.** *Upper*: Representative traces for G_{in} before (black) and 25 min after MF conditioning
785 (upper) in CA3-PCs of ZnT3HT mice. *Lower*: Summary for G_{in} before and after 50 Hz MF conditioning in
786 CA3-PCs from ZnT3HT mice (n = 5, t = -1.141, p = 0.318, paired t-test). **B.** Timeline of experimental
787 procedure. **Ca.** G_{in} before and after 10 Hz 2 s somatic conditioning in CA3-PCs of ZnT3-HT/cfos-shEGFP
788 mice (black),. G_{in} before and after somatic conditioning in other groups of CA3-PCs were reproduced from
789 previous figure (Fig. 6, the same but pale colour codes). **Cb.** Representative traces for G_{in} before (black)
790 and 25 min after conditioning (*upper*) and summary of G_{in} before and after somatic conditioning in CA3-
791 PCs from ZnT3HT/cfos-shEGFP mice (n = 6, t = 7.675, p = 0.001, paired t-test). **Da-b.** Baseline G_{in} (*Ca*) and
792 post/pre-conditioning G_{in} ratio (*Cb*) as a function of G/R ratio in CA3-PCs of ZnT3-HT/cfos-shEGFP mice
793 (black). Colored symbols are reproduced from Fig. 6 with pale color.

794 *Fig. 8*

795 **Fig. 8 Input-specific bi-directional regulation of intrinsic excitability may contribute to sequential**
796 **memories. A.** Schematic illustration of CA3 network model comprised of pyramidal cells (PCs, black
797 triangles) and an inhibitory interneuron (IN, green circle). **Ba.** Input patterns via MF (red dots) and PP (blue
798 dots) during encoding phase. Inset, broken boxed region in an expanded scale. **Bb**. Raster plot of network
799 responses to the input patterns shown in Ba. The distributions for the number of MF and PP inputs per a
800 pattern are shown in Fig. S7D. The cell indices of 1 to 1000 are PCs, and the rest cell indices (1001 ~ 1200)
801 are INs. **C,** Ca^{2+} (blue) and Zn^{2+} (red) transients in a PC in the $\mathbf{M_1}$ subset (cell id = 96) during the encoding
802 phase. The timings of input pattern arrival are indicated by arrows below the abscissa. The intrinsic
803 excitability index (IE, green broken line) starts to increase when both [Ca^{2+}] and [Zn^{2+}] are higher than their
804 thresholds (Caθ1 = 1.5 a.u.; Znθ = 3 a.u.). When IE > 0.7, the arrival of subsequent PP inputs elicits a CaT
805 devoid of Zn^{2+} signaling. When CaTs is higher than Caθ2 (= 0.9 a.u.) without Zn^{2+} signal, the IE returns to
806 the baseline. Afterwards, this PC does not fire any longer in response to PP inputs alone. Note that the
807 kinetics of Ca^{2+}, Zn^{2+} and IE were assumed faster than real values for the sake of reducing computing time
808 (decay τ for CaT and ZnT = 150 and 300 ms, respectively; rise and decay τ for IE = 150 and 50 ms,
809 respectively). **D.** Part of matrix of A/C synaptic weights (boxed in the Inset) resulting from training the
810 recurrent network using a series of 4 patterns shown in Ba. Rows and columns represent indices of post-
811 and pre-synaptic CA3-PCs, respectively. Synaptic weights are color-coded as shown on the right bar. Note
812 that sparse potentiation of synaptic weights between $\mathbf{M_1}$ (cell index, 1-200) and $\mathbf{M_2}$ (cell index, 201-400)
813 but not between $\mathbf{M_1}$ and $\mathbf{M_3}$ (cell index, 401-600). **E**, *Left*, Raster plot of network responses to the PP inputs
814 shown in Fig. S7E. Note that most PP inputs are terminated in 30 ms (Fig. S7E), but the complete recall of

815 **M_1** is accomplished by recurrent connections that have been strengthened during encoding phase. In turn,
816 hetero-association between **M_1** and **M_2** that occurred during encoding phase allows subsequent activation
817 of **M_2**, and so on. Right, cumulative fraction of activated PCs in each ensemble.

818

References

Bennett, M. R., Gibson, W. G., & Robinson, J. (1994). Dynamics of the CA3 pyramidal neuron autoassociative memory network in the hippocampus *Philos Trans R Soc Lond B Biol Sci*, *29*, 11.

Blanchetot, C., Tertoolen, L. G., & den Hertog, J. (2002). Regulation of receptor protein-tyrosine phosphatase alpha by oxidative stress. . *The EMBO journal*, *21*(4), 11. https://doi.org/https://doi.org/10.1093/emboj/21.4.493

Brandt, D., Goerke, A., Heuer, M., Gimona, M., Leitges, M., Kremmer, E., . . . Mischak, H. (2003). Protein kinase C delta induces Src kinase activity via activation of the protein tyrosine phosphatase PTP alpha. *J Biol Chem*, *278*(36), 34073-34078. https://doi.org/10.1074/jbc.M211650200

Buzsaki, G., & Mizuseki, K. (2014). The log-dynamic brain: how skewed distributions affect network operations. *Nat Rev Neurosci*, *15*(4), 264-278. https://doi.org/10.1038/nrn3687

Cai, D. J., Aharoni, D., Shuman, T., Shobe, J., Biane, J., Song, W., . . . Silva, A. J. (2016). A shared neural ensemble links distinct contextual memories encoded close in time. *Nature*, *534*(7605), 115-118. https://doi.org/10.1038/nature17955

Chen, X., Yuan, L. L., Zhao, C., Birnbaum, S. G., Frick, A., Jung, W. E., . . . Johnston, D. (2006). Deletion of Kv4.2 gene eliminates dendritic A-type K+ current and enhances induction of long-term potentiation in hippocampal CA1 pyramidal neurons. *J Neurosci*, *26*(47), 12143-12151. https://doi.org/10.1523/JNEUROSCI.2667-06.2006

Dong, Y., Green, T., Saal, D., Marie, H., Neve, R., Nestler, E. J., & Malenka, R. C. (2006). CREB modulates excitability of nucleus accumbens neurons. *Nat Neurosci*, *9*(4), 475-477. https://doi.org/10.1038/nn1661

Eom, K., Hyun, J. H., Lee, D. G., Kim, S., Jeong, H. J., Kang, J. S., . . . Lee, S. H. (2019). Intracellular Zn(2+) Signaling Facilitates Mossy Fiber Input-Induced Heterosynaptic Potentiation of Direct Cortical Inputs in Hippocampal CA3 Pyramidal Cells. *J Neurosci*, *39*(20), 3812-3831. https://doi.org/10.1523/JNEUROSCI.2130-18.2019

Eom, K., Lee, H. R., Hyun, J. H., An, H., Lee, Y. S., Ho, W. K., & Lee, S. H. (2022). Gradual decorrelation of CA3 ensembles associated with contextual discrimination learning is impaired by Kv1.2 insufficiency. *Hippocampus*, *32*(3), 193-216. https://doi.org/10.1002/hipo.23400

Farovik, A., Dupont, L. M., & Eichenbaum, H. (2010). Distinct roles for dorsal CA3 and CA1 in memory for sequential nonspatial events. *Learn Mem*, *17*(1), 12-17. https://doi.org/10.1101/lm.1616209

Forman, H. J., Zhang, H., & Rinna, A. (2009). Glutathione: overview of its protective roles, measurement, and biosynthesis. *Mol Aspects Med*, *30*(1-2), 1-12. https://doi.org/10.1016/j.mam.2008.08.006

Garcia, A. J., 3rd, Putnam, R. W., & Dean, J. B. (2010). Hyperoxic stimulation of synchronous orthodromic activity and induction of neural plasticity does not require changes in excitatory synaptic transmission. *J Appl Physiol (1985)*, *109*(3), 820-829. https://doi.org/10.1152/japplphysiol.91430.2008

Grishin, A. A., Benquet, P., & Gerber, U. (2005). Muscarinic receptor stimulation reduces NMDA responses in CA3 hippocampal pyramidal cells via Ca2+-dependent activation of tyrosine phosphatase. *Neuropharmacology*, *49*(3), 328-337. https://doi.org/10.1016/j.neuropharm.2005.03.019

Guzman, S., Schlögl, A., Frotscher, M., & Jonas, P. (2016). Synaptic mechanisms of pattern completion in the hippocampal CA3 network. *Science*, *353*, 1117-1123.

Hasselmo, M. E. (2006). The role of acetylcholine in learning and memory. *Curr Opin Neurobiol*, *16*(6), 710-715. https://doi.org/10.1016/j.conb.2006.09.002

Henze, D., Wittner, L., & Buzsaki, G. (2002). Single granule cells reliably discharge targets in the hippocampal CA3 network in vivo. *Nat Neurosci*, *5*(8), 790-795. https://doi.org/10.1038/nn887

Hunsaker, M. R., & Kesner, R. P. (2013). The operation of pattern separation and pattern completion processes associated with different attributes or domains of memory. *Neurosci Biobehav Rev*, *37*(1), 36-58. https://doi.org/10.1016/j.neubiorev.2012.09.014

Hurvich, C. M., & Tsai, C. L. (1989). Regression and Time-Series Model Selection in Small Samples. *Biometrika*, *76*(2), 297-307. https://doi.org/DOI 10.1093/biomet/76.2.297

Hyun, J., Eom, K., Lee, K., Bae, J., Bae, Y., Kim, M., . . . Lee, S. (2015). Kv1.2 mediates heterosynaptic modulation of direct cortical synaptic inputs in CA3 pyramidal cells. *J Physiol*, *593*(16), 3617-3643. https://doi.org/10.1113/JP270372

Hyun, J., Eom, K., Lee, K., Ho, W., & Lee, S. (2013). Activity-dependent downregulation of D-type K+ channel subunit Kv1.2 in rat hippocampal CA3 pyramidal neurons. *J Physiol*, *591*(22), 5525-5540. https://doi.org/10.1113/jphysiol.2013.259002

Ikegaya, Y., Sasaki, T., Ishikawa, D., Honma, N., Tao, K., Takahashi, N., . . . Matsuki, N. (2013). Interpyramid spike transmission stabilizes the sparseness of recurrent network activity. *Cereb Cortex*, *23*(2), 293-304. https://doi.org/10.1093/cercor/bhs006

Jahnke, S., Timme, M., & Memmesheimer, R. M. (2015). A Unified Dynamic Model for Learning, Replay, and Sharp-Wave/Ripples. *J Neurosci*, *35*(49), 16236-16258. https://doi.org/10.1523/JNEUROSCI.3977-14.2015

Jonas, P., Major, G., & Sakmann, B. (1993). Quantal components of unitary EPSCs at the mossy fibre synapse on CA3 pyramidal cells of rat hippocampus. *J Physiol.*, *472*, 49.

Kastellakis, G., Silva, A. J., & Poirazi, P. (2016). Linking Memories across Time via Neuronal and Dendritic Overlaps in Model Neurons with Active Dendrites. *Cell Rep*, *17*(6), 1491-1504. https://doi.org/10.1016/j.celrep.2016.10.015

Kohus, Z., Kali, S., Rovira-Esteban, L., Schlingloff, D., Papp, O., Freund, T. F., . . . Gulyas, A. I. (2016). Properties and dynamics of inhibitory synaptic communication within the CA3 microcircuits of pyramidal cells and interneurons expressing parvalbumin or cholecystokinin. *J Physiol*, *594*(13), 3745-3774. https://doi.org/10.1113/JP272231

Kowalski, J., Gan, J., Jonas, P., & Pernia-Andrade, A. J. (2016). Intrinsic membrane properties determine hippocampal differential firing pattern in vivo in anesthetized rats. *Hippocampus*, *26*(5), 668-682. https://doi.org/10.1002/hipo.22550

Lee, D., Hyun, J. H., Jung, K., Hannan, P., & Kwon, H. B. (2017). A calcium- and light-gated switch to induce gene expression in activated neurons. *Nat Biotechnol*, *35*(9), 858-863. https://doi.org/10.1038/nbt.3902

Lee, I., & Kesner, R. P. (2004). Encoding versus retrieval of spatial memory: Double dissociation between the dentate gyrus and the perforant path inputs into CA3 in the dorsal hippocampus. *Hippocampus*, *14*(1), 66-76. https://doi.org/DOI 10.1002/hipo.10167

Lev, S., Moreno, H., Martinez , R., Canoll, P., Peles, E., Musacchio, J., . . . Schlessinger, J. (1995). Protein tyrosine kinase PYK2 involved in Ca2+-induced regulation of ion channel and MAP kinase functions. *Nature*, *376*, 737-745.

Levy, W. B., Hocking, A. B., & Wu, X. (2005). Interpreting hippocampal function as recoding and forecasting. *Neural Networks*, *18*, 23.

Lisman, J., Cooper, K., Sehgal, M., & Silva, A. J. (2018). Memory formation depends on both synapse-specific modifications of synaptic strength and cell-specific increases in excitability. *Nat Neurosci*, *21*(3), 309-314. https://doi.org/10.1038/s41593-018-0076-6

Lopez de Armentia, M., Jancic, D., Olivares, R., Alarcon, J. M., Kandel, E. R., & Barco, A. (2007). cAMP response element-binding protein-mediated gene expression increases the intrinsic excitability of

CA1 pyramidal neurons. *J Neurosci*, *27*(50), 13909-13918. https://doi.org/10.1523/JNEUROSCI.3850-07.2007

Malezieux, M., Kees, A. L., & Mulle, C. (2020). Theta Oscillations Coincide with Sustained Hyperpolarization in CA3 Pyramidal Cells, Underlying Decreased Firing. *Cell Rep*, *32*(1), 107868. https://doi.org/10.1016/j.celrep.2020.107868

McMahon, D., & Barrionuevo, G. (2002). Short- and long-term plasticity of the perforant path synapse in hippocampal area CA3. *J Neurophysiol*, *88*, 528-533.

McNaughton, B. L., & Morris, R. G. (1987). Hippocampal synaptic enhancement and information storage within a distributed memory system. *Trends in neurosciences*, *10*(10), 8.

Meng, T., Fukada, T., & Tonks, N. (2002). Reversible oxidation and inactivation of protein tyrosine phosphatases in vivo. . *Mol Cell*, *9*(2), 13. https://doi.org/https://doi.org/10.1016/s1097-2765(02)00445-8

Mishra, R. K., Kim, S., Guzman, S. J., & Jonas, P. (2016). Symmetric spike timing-dependent plasticity at CA3-CA3 synapses optimizes storage and recall in autoassociative networks. *Nat Commun*, *7*, 11552. https://doi.org/10.1038/ncomms11552

Moeyaert, B., Holt, G., Madangopal, R., Perez-Alvarez, A., Fearey, B. C., Trojanowski, N. F., . . . Schreiter, E. R. (2018). Improved methods for marking active neuron populations. *Nat Commun*, *9*(1), 4440. https://doi.org/10.1038/s41467-018-06935-2

Moser, E. I., Krobert, K. A., Moser, M. B., & Morris, R. G. (1998). Impaired spatial learning after saturation of long-term potentiation. *Science*, *281*(5385), 2038-2042. https://doi.org/10.1126/science.281.5385.2038

O'Reilly, R. C., & McClelland, J. L. (1994). Hippocampal conjunctive encoding, storage, and recall: avoiding a trade-off. *Hippocampus*, *4*, 661-682.

Oh, M. M., & Disterhoft, J. F. (2015). Increased Excitability of Both Principal Neurons and Interneurons during Associative Learning. *Neuroscientist*, *21*(4), 372-384. https://doi.org/10.1177/1073858414537382

Perez-Rosello, T., Baker, J., Ferrante, M., Iyengar, S., Ascoli, G., & Barrionuevo, G. (2011). Passive and active shaping of unitary responses from associational/commissural and perforant path synapses in hippocampal CA3 pyramidal cells. . *J Comp Neurosci 31,* , 159-182. https://doi.org/10.1007/s10827-010-0303-y)

Pignatelli, M., Ryan, T. J., Roy, D. S., Lovett, C., Smith, L. M., Muralidhar, S., & Tonegawa, S. (2019). Engram Cell Excitability State Determines the Efficacy of Memory Retrieval. *Neuron*, *101*(2), 274-284 e275. https://doi.org/10.1016/j.neuron.2018.11.029

Rashid, A. J., Yan, C., Mercaldo, V., Hsiang, H. L., Park, S., Cole, C. J., . . . Josselyn, S. A. (2016). Competition between engrams influences fear memory formation and recall. *Science*, *353*(6297), 383-387. https://doi.org/10.1126/science.aaf0594

Shigemoto, R., Kinoshita, A., Wada, E., Nomura, S., Ohishi, H., Takada, M., . . . Mizuno, N. (1997). Differential Presynaptic Localization of Metabotropic Glutamate Receptor Subtypes in the Rat Hippocampus. *The Journal of neuroscience*, *17*(19), 20.

Silva, A. J., Zhou, Y., Rogerson, T., Shobe, J., & Balaji, J. (2009). Molecular and cellular approaches to memory allocation in neural circuits. *Science*, *326*(5951), 391-395. https://doi.org/10.1126/science.1174519

Sorensen, A. T., Cooper, Y. A., Baratta, M. V., Weng, F. J., Zhang, Y., Ramamoorthi, K., . . . Lin, Y. (2016). A robust activity marking system for exploring active neuronal ensembles. *Elife*, *5*. https://doi.org/10.7554/eLife.13918

Treves, A., & Rolls, E. (1992). Computational constraints suggest the need for two distinct input systems to the hippocampal CA3 network. . *Hippocampus*, *2*, 189-199.

957 Tsai, W., Morielli, A., Cachero, T., & Peralta, E. (1998). Receptor protein tyrosine phosphatase alpha
958 participates in the m1 muscarinic acetylcholine receptor-dependent regulation of Kv1.2 channel
959 activity. *EMBO*, *18,*, 109-118.
960 Tsukamoto, M., Yasui, T., Yamada, M. K., Nishiyama, N., Matsuki, N., & Ikegaya, Y. (2003). Mossy fibre
961 synaptic NMDA receptors trigger non-hebbian long-term potentiation at entorhino-CA3 synapses
962 in the rat. *The Journal of Physiology*, *546*(3), 665-675.
963 https://doi.org/10.1113/jphysiol.2002.033803
964 Vogt, K., & Regehr, W. (2001). Cholinergic modulation of excitatory synaptic transmission in the CA3 area
965 of the hippocampus. *The Journal of neuroscience*, *21*(1), 9.
966 https://doi.org/https://doi.org/10.1523/JNEUROSCI.21-01-00075.2001
967 Wallenstein, G. V., Eichenbaum, H., & Hasselmo, M. E. (1998). The hippocampus as an associator of
968 discontiguous events *Trends Neurosci*, *21*, 7.
969 Yoon, J. Y., Lee, H. R., Ho, W. K., & Lee, S. H. (2020). Disparities in Short-Term Depression Among Prefrontal
970 Cortex Synapses Sustain Persistent Activity in a Balanced Network. *Cereb Cortex*, *30*(1), 113-134.
971 https://doi.org/10.1093/cercor/bhz076

972

Fig. 1

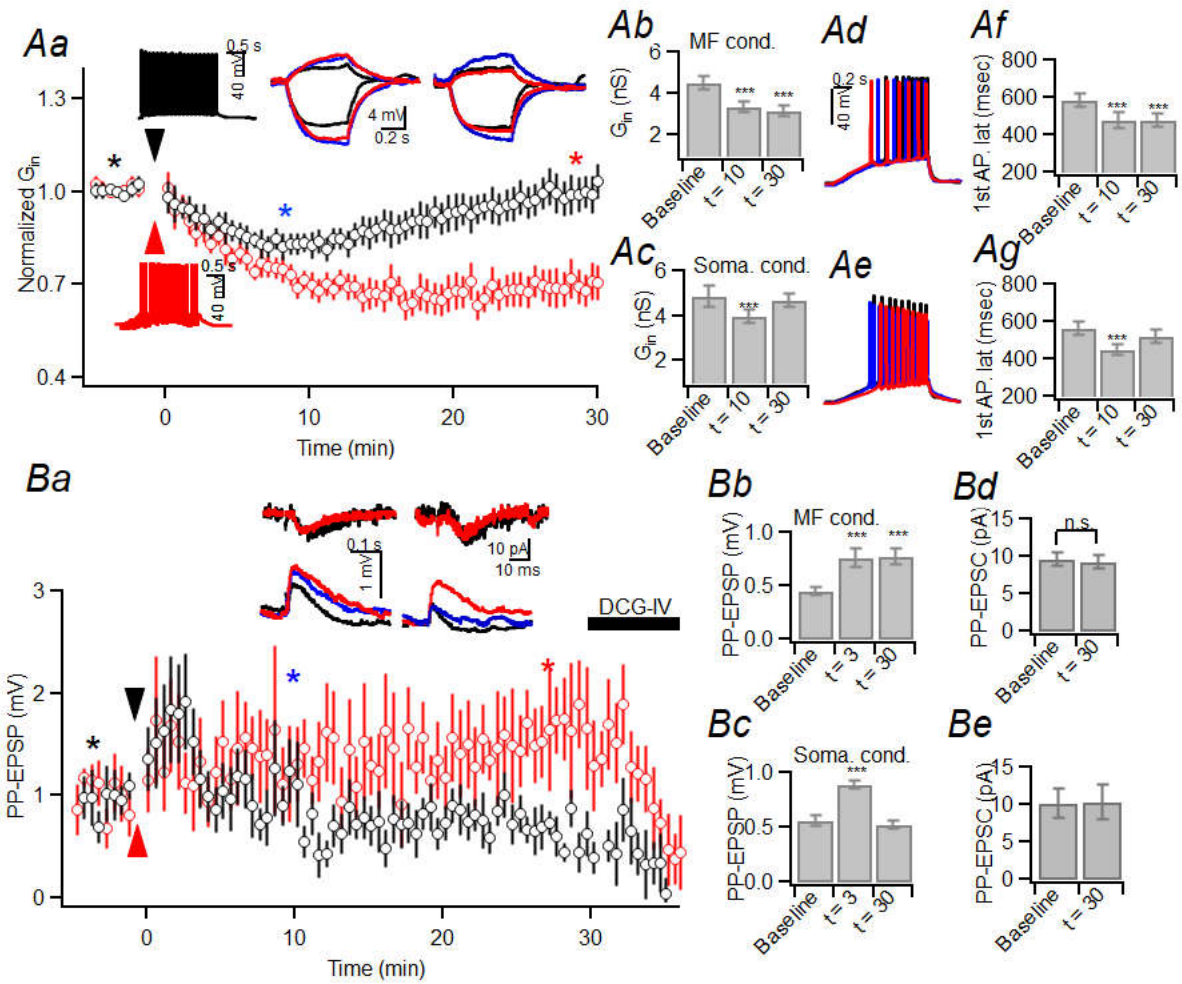
Aa
Normalized G_{in}
Time (min)
0.5 s
40 mV
4 mV
0.2 s
Ab
MF cond.
G_{in} (nS)
Baseline
t = 10
t = 30
Ac
Soma. cond.
Ad
Ae
Af
1st AP. lat (msec)
Ag
Ba
PP-EPSP (mV)
0.1 s
1 mV
10 pA
10 ms
DCG-IV
Bb
MF cond.
t = 3
Bc
Soma. cond.
Bd
PP-EPSC (pA)
n.s.
Be

Fig. 2

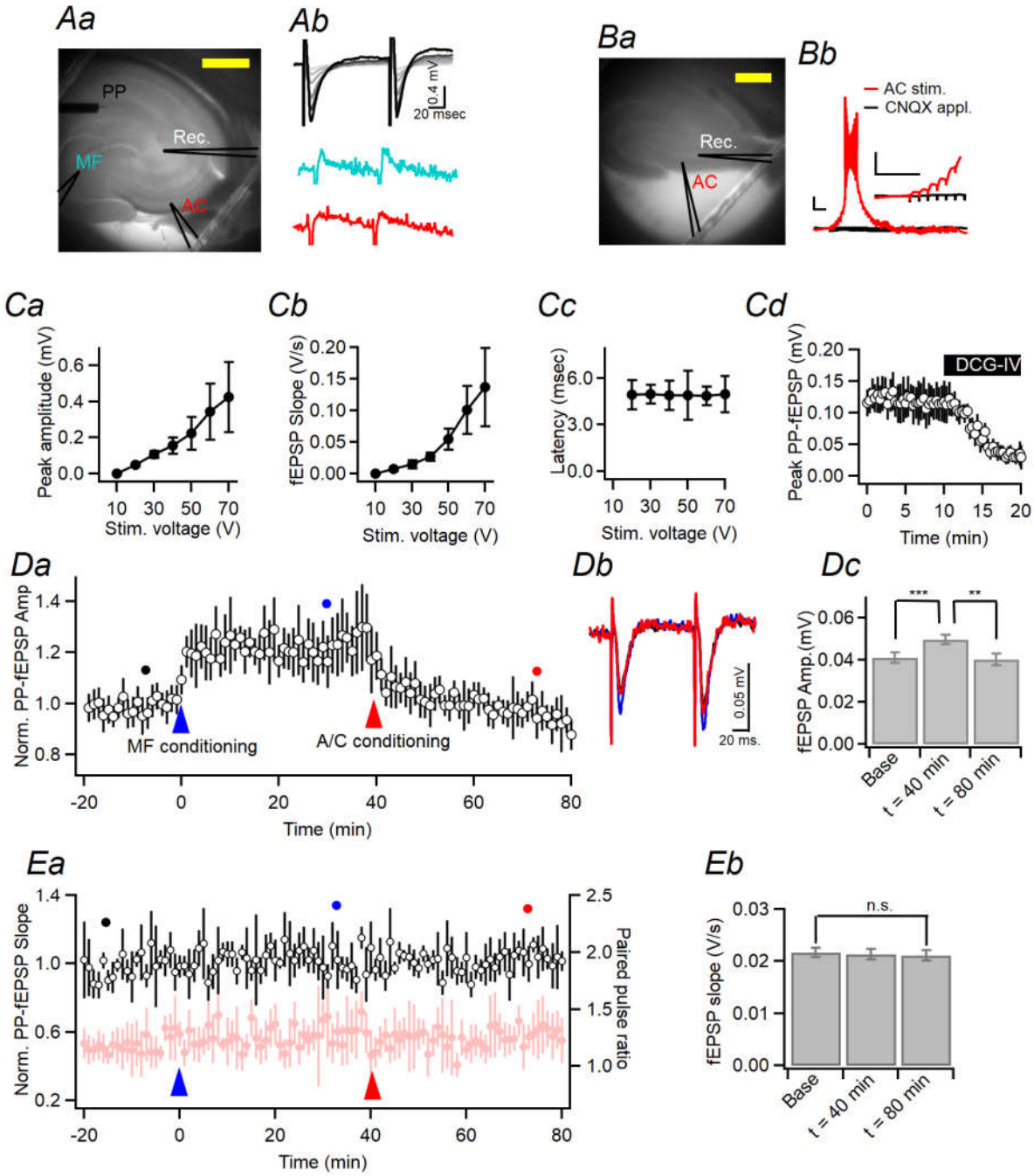
Aa
PP
Rec.
MF
AC
Ab
0.4 mV
20 msec
Ba
Rec.
AC
Bb
AC stim.
CNQX appl.
Ca
Peak amplitude (mV)
Stim. voltage (V)
Cb
fEPSP Slope (V/s)
Stim. voltage (V)
Cc
Latency (msec)
Stim. voltage (V)
Cd
Peak PP-fEPSP (mV)
DCG-IV
Time (min)
Da
Norm. PP-fEPSP Amp
MF conditioning
A/C conditioning
Time (min)
Db
0.05 mV
20 ms.
Dc
fEPSP Amp.(mV)
Base
t = 40 min
t = 80 min
Ea
Norm. PP-fEPSP Slope
Paired pulse ratio
Time (min)
Eb
fEPSP slope (V/s)
n.s.
Base
t = 40 min
t = 80 min

Fig. 3

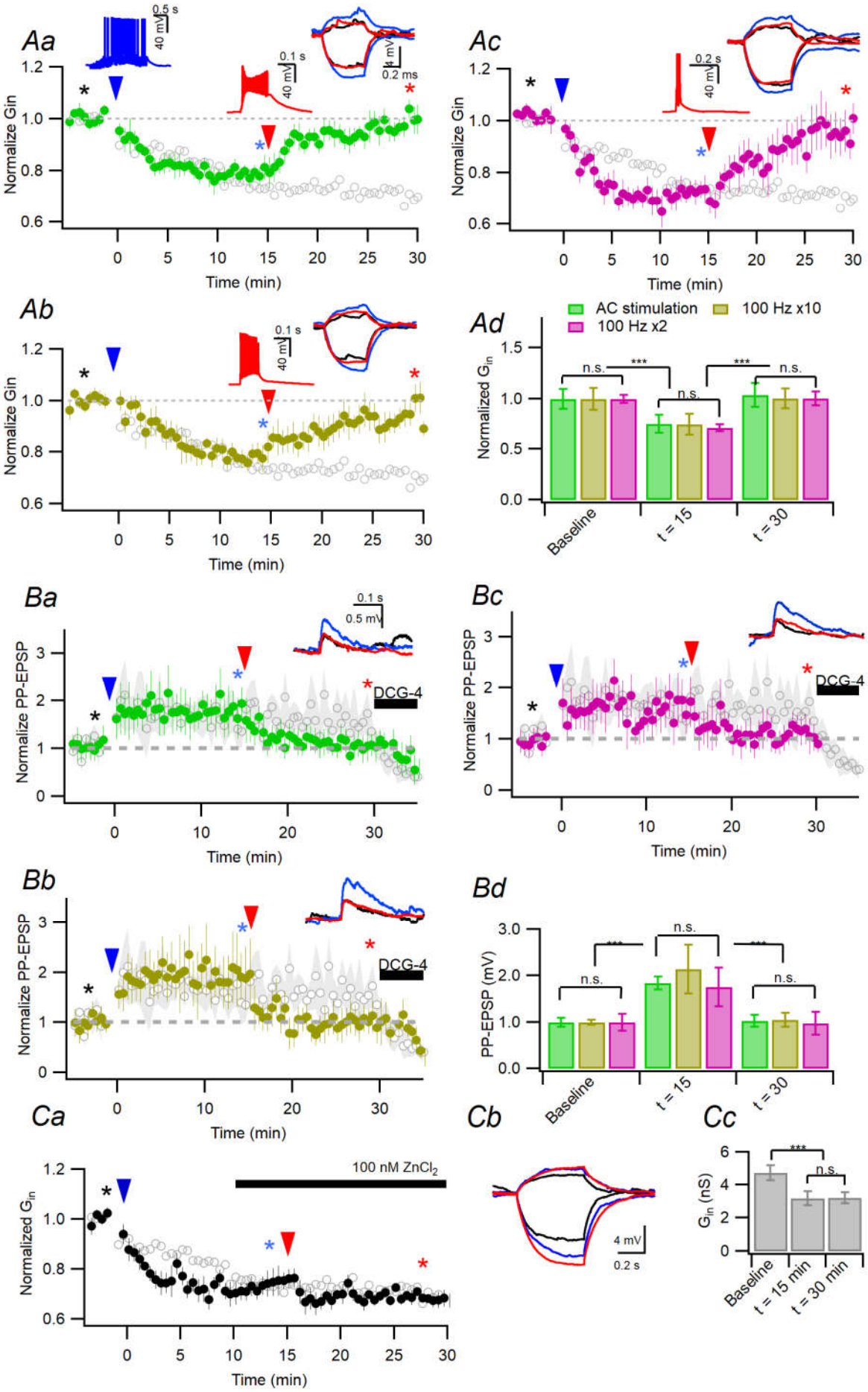
Aa
Ac
Ab
Ad
Ba
Bc
Bb
Bd
Ca
Cb
Cc
Normalize Gin
Normalized Gin
Normalize PP-EPSP
PP-EPSP (mV)
Time (min)
AC stimulation
100 Hz x10
100 Hz x2
Baseline
t = 15
t = 30
DCG-4
100 nM ZnCl2
Gin (nS)
t = 15 min
t = 30 min
n.s.
***

Fig. 4

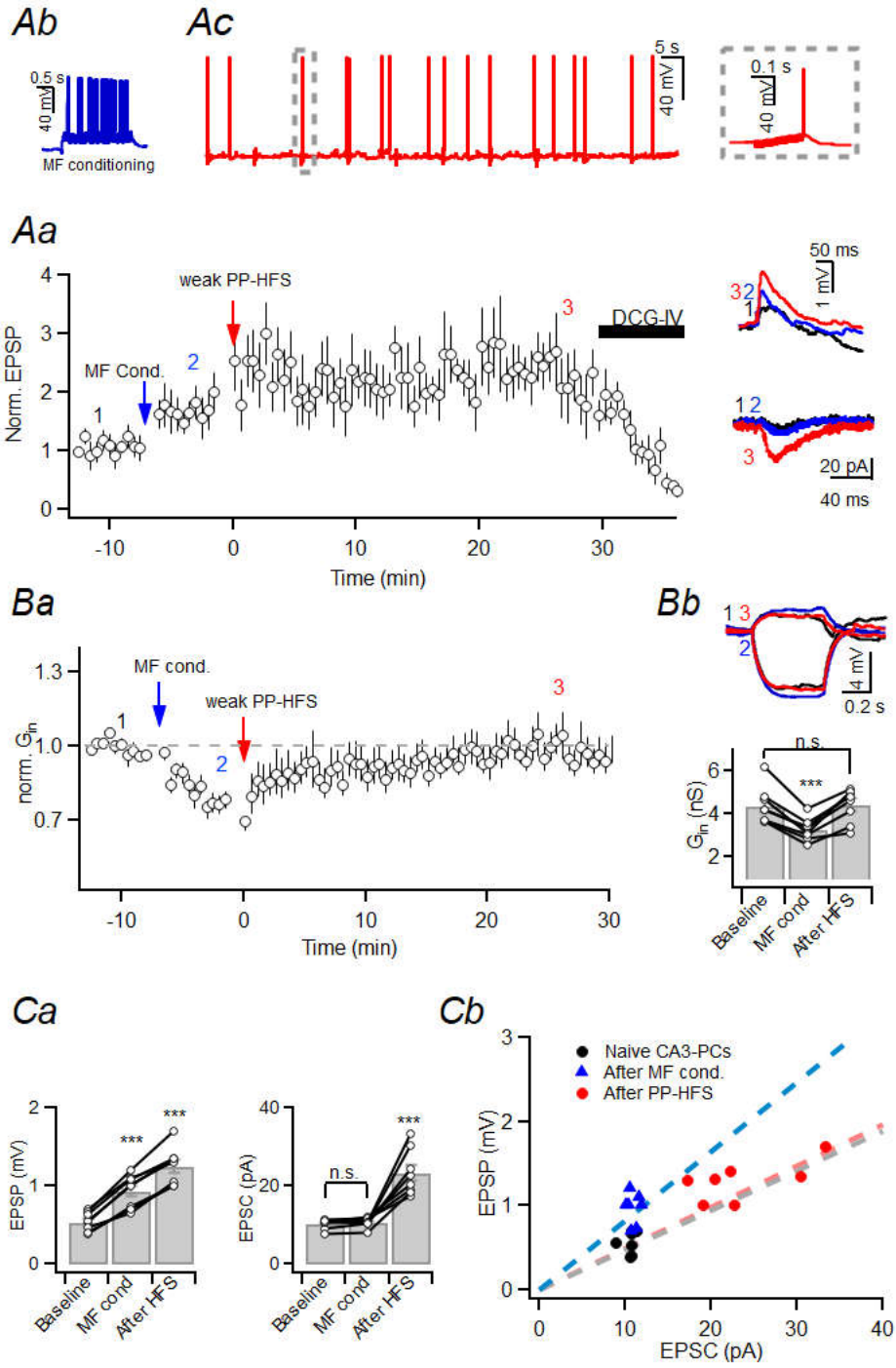
Ab
Ac
0.5 s
40 mV
MF conditioning
5 s
40 mV
0.1 s
40 mV
Aa
weak PP-HFS
MF Cond.
DCG-IV
Norm. EPSP
Time (min)
50 ms
1 mV
20 pA
40 ms
Ba
MF cond.
weak PP-HFS
norm. G_{in}
Time (min)
Bb
4 mV
0.2 s
n.s.
***
G_{in} (nS)
Baseline
MF cond
After HFS
Ca
EPSP (mV)
EPSC (pA)
n.s.
Cb
Naive CA3-PCs
After MF cond.
After PP-HFS
EPSP (mV)
EPSC (pA)

Fig. 5

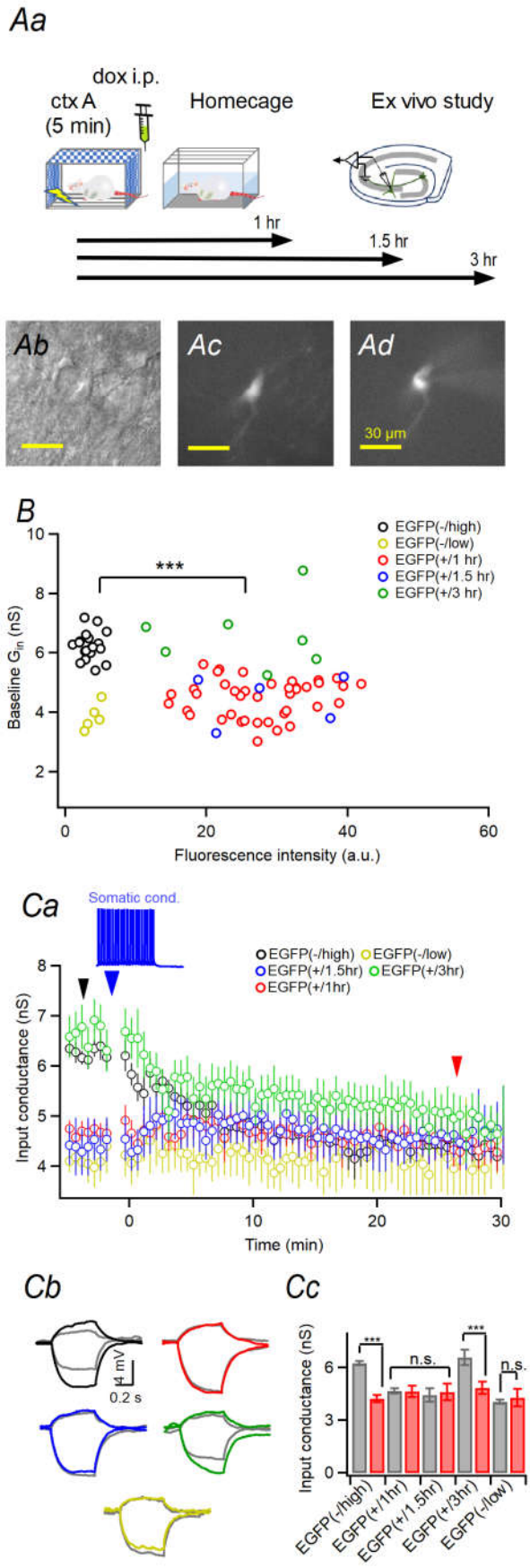
Aa
dox i.p.
ctx A
(5 min)
Homecage
Ex vivo study
1 hr
1.5 hr
3 hr
Ab
Ac
Ad
30 μm
B
EGFP(-/high)
EGFP(-/low)
EGFP(+/1 hr)
EGFP(+/1.5 hr)
EGFP(+/3 hr)
***
Baseline G_m (nS)
Fluorescence intensity (a.u.)
Ca
Somatic cond.
EGFP(-/high)
EGFP(-/low)
EGFP(+/1.5hr)
EGFP(+/3hr)
EGFP(+/1hr)
Input conductance (nS)
Time (min)
Cb
4 mV
0.2 s
Cc
***
n.s.
***
n.s.
Input conductance (nS)
EGFP(-/high)
EGFP(+/1hr)
EGFP(+/1.5hr)
EGFP(+/3hr)
EGFP(-/low)

Fig. 6

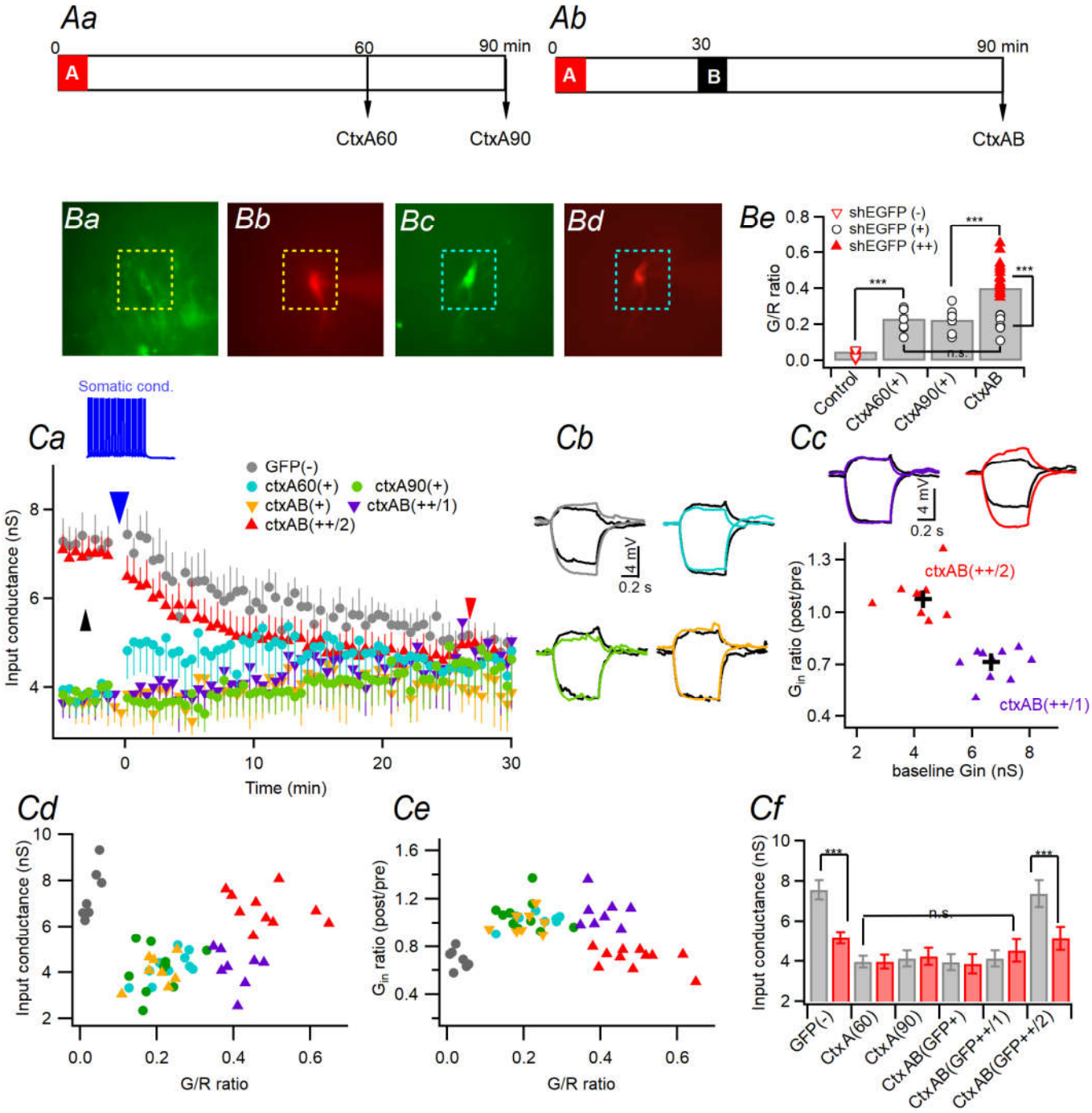
Aa
0
60
90 min
A
CtxA60
CtxA90
Ab
0
30
90 min
A
B
CtxAB
Ba
Bb
Bc
Bd
Be
shEGFP (-)
shEGFP (+)
shEGFP (++)
G/R ratio
Control
CtxA60(+)
CtxA90(+)
CtxAB
n.s.
Somatic cond.
Ca
GFP(-)
ctxA60(+)
ctxA90(+)
ctxAB(+)
ctxAB(++/1)
ctxAB(++/2)
Input conductance (nS)
Time (min)
Cb
4 mV
0.2 s
Cc
4 mV
0.2 s
ctxAB(++/2)
ctxAB(++/1)
Gin ratio (post/pre)
baseline Gin (nS)
Cd
Input conductance (nS)
G/R ratio
Ce
Gin ratio (post/pre)
G/R ratio
Cf
Input conductance (nS)
n.s.
GFP(-)
CtxA(60)
CtxA(90)
CtxAB(GFP+)
CtxAB(GFP++/1)
CtxAB(GFP++/2)

Fig. 7

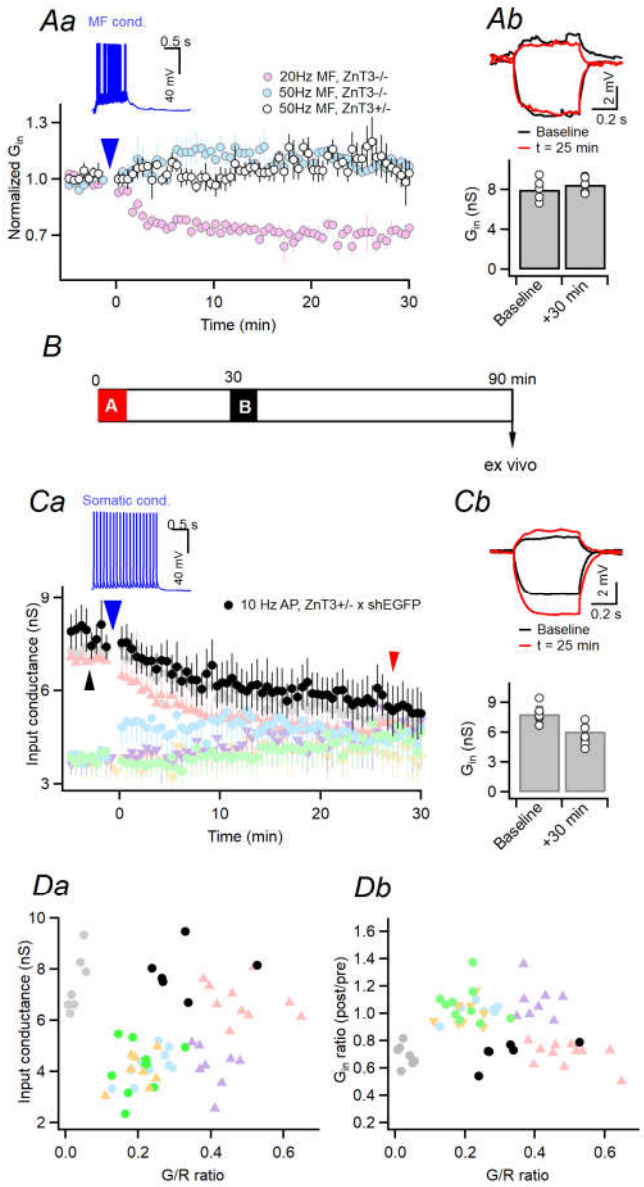
Aa
MF cond.
0.5 s
40 mV
20Hz MF, ZnT3-/-
50Hz MF, ZnT3-/-
50Hz MF, ZnT3+/-
Normalized G_{in}
Time (min)
Ab
2 mV
0.2 s
Baseline
t = 25 min
G_{in} (nS)
Baseline
+30 min
B
0
30
90 min
A
B
ex vivo
Ca
Somatic cond.
0.5 s
40 mV
10 Hz AP, ZnT3+/- x shEGFP
Input conductance (nS)
Time (min)
Cb
2 mV
0.2 s
Baseline
t = 25 min
G_{in} (nS)
Baseline
+30 min
Da
Input conductance (nS)
G/R ratio
Db
G_{in} ratio (post/pre)
G/R ratio

Fig. 8

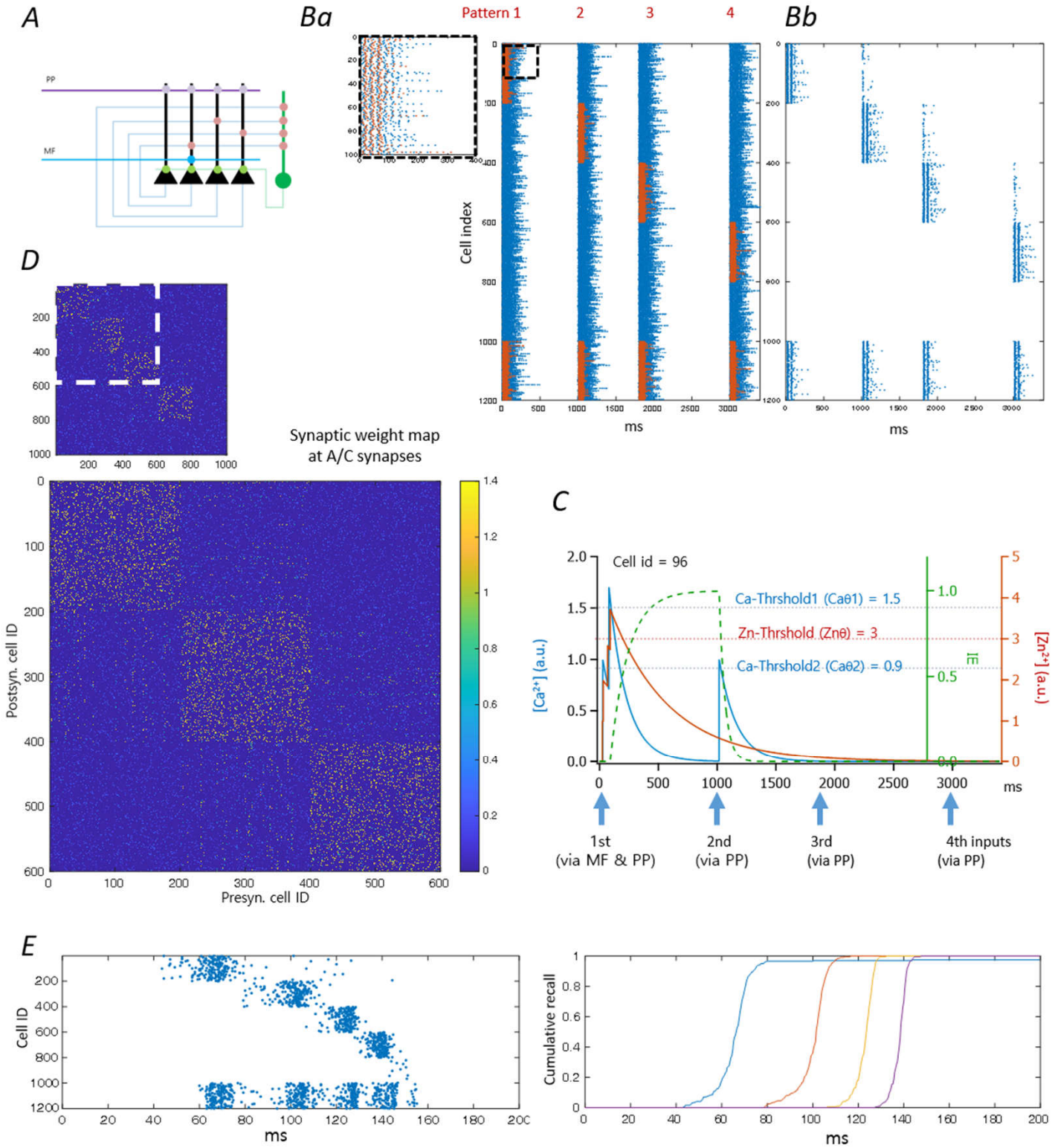
A
PP
MF
Ba
Pattern 1
2
3
4
Cell index
ms
Bb
ms
D
Synaptic weight map
at A/C synapses
Postsyn. cell ID
Presyn. cell ID
C
Cell id = 96
Ca-Thrshold1 (Caθ1) = 1.5
Zn-Thrshold (Znθ) = 3
Ca-Thrshold2 (Caθ2) = 0.9
[Ca2+] (a.u.)
[Zn2+] (a.u.)
ms
1st
(via MF & PP)
2nd
(via PP)
3rd
(via PP)
4th inputs
(via PP)
E
Cell ID
ms
Cumulative recall
ms